

THESIS FOR THE DEGREE OF LICENTIATE OF ENGINEERING

**Simulation of Irregular Waves and Wave Induced Loads on
Wind Power Plants in Shallow Water**

JENNY TRUMARS



Department of Water Environment Transport
CHALMERS UNIVERSITY OF TECHNOLOGY
Göteborg, Sweden 2003

Simulation of Irregular Waves and Wave Induced Loads on Wind Power Plants in
Shallow Water

JENNY TRUMARS

© Jenny Trumars, 2003

Doktorsavhandlingar och licentiatuppsatser på Vatten Miljö Transport, nr 7
ISSN 1650-4143

Department of Water Environment Transport
Chalmers University of Technology
S-412 96 Göteborg
Sweden
Telephone +46(0)31 772 1000

Chalmers reproservice
Göteborg, Sweden 2003

Simulation of Irregular Waves and Wave Induced Loads on Wind Power Plants in Shallow Water

JENNY TRUMARS

Department of Water Environment Transport
Chalmers University of Technology

Abstract

The essay gives a short introduction to waves and discusses the problem with non-linear waves in shallow water and how they effect an offshore wind energy converter. The focus is on the realisation of non-linear waves in the time domain from short-term statistics in the form of a variance density spectrum of the wave elevation. For this purpose the wave transformation from deep water to the near to shore site of a wind energy farm at Bockstigen has been calculated with the use of SWAN (Simulating WAVes Near Shore). The result is a wave spectrum, which can be used as input to the realisation. The realisation of waves is done by perturbation theory to the first and second-order. The properties calculated are the wave elevation, water particle velocity and acceleration.

The wave heights from the second order perturbation equations are higher than those from the first order perturbation equations. This is also the case for the water particle kinematics. The increase of variance is significant between the first order and the second order realisation. The calculated wave elevation exhibits non-linear features as the peaks become sharper and the troughs flatter.

The resulting forces are calculated using Morison's equation. For second order force and base moment there is an increase in the maximum values. The force and base moment are largest approximately at the zero up and down crossing of the wave elevation. This indicates an inertia dominated wave load.

So far the flexibility and the response of the structure have not been taken into account. They are, however, of vital importance.

For verification of the wave model the results will later on be compared with measurements at Bockstigen off the coast of Gotland in the Baltic Sea.

Keywords: Non-linear wave models, wind energy converter, shallow water, perturbation theory, ocean engineering, wave load.

Simulation of Irregular Waves and Wave Induced Loads on Wind Power Plants in Shallow Water

JENNY TRUMARS

Institutionen för Vatten miljö transport
Chalmers tekniska högskola

Sammanfattning

Uppsatsen ger en kort introduktion till vågor och behandlar sedan problemet med icke-linjära vågor på grunt vatten och hur de påverkar ett vindkraftverk till havs. Focus för arbetet är på realiseringen av icke-linjära vågor i tiden från korttidsstatistik i form av variansspektrum över vågornas elevation. För detta ändamål har vågtransformationen från djupt vatten till det grundare vattnet som vindkraftsparken vid Bockstigen står i beräknats i SWAN (Simulating WAves Near Shore). Resultatet är ett vågspektrum som kan användas som input till realiseringen. Realiseringen görs med en perturbationsteori till första och andra ordningen. De beräknade egenskaperna är vågelevationen, partikelhastigheterna och partikelaccelerationerna.

Våghöjderna beräknade med andra ordningens perturbationsekvationer är högre än för de beräknade med första ordningens perturbationsekvationer. Detta är även fallet för vattnets partikelkinematik. Variansen ökar kraftigt för andra ordningens realisation. Den beräknade våghöjden uppvisar icke-linjära egenskaper som att vågtopparna blir skarpare och vågdalarna flackare.

De resulterande krafterna beräknas med Morisons ekvation. För andra ordningens realisation ökar kraftens och basmomentets maxvärden. Kraften och momentet är störst vid nollkryssningsperioderna för vågelevationen. Detta tyder på att belastningen är mass-tröghetsdominerad.

Inverkan av strukturens flexibilitet på dess respons har ännu inte studerats. Flexibiliteten hos strukturen och dämpningen i grundläggningen är dock av stor betydelse.

För verifiering av vågmodellen ska resultaten senare jämföras med mätningar utanför Bockstigen vid Gotland kust.

Nyckelord: Ickelinjära vågmodeller, vindkraftverk, grunt vatten, perturbationsteori, havsteknik

List of Appended Papers

This thesis is based on the work contained in the following papers, which are referred to in the text.

Paper A:

Jenny Trumars, Johan Jonsson and Lars Bergdahl,
Extreme Non-Linear Wave Forces on a Monopile in Shallow water,
In: Proceedings of OMAE03, 22ND International Conference on Offshore Mechanics and Arctic Engineering, June 8–13, 2003, Cancun, Mexico

Paper B:

Jenny Trumars, Johan Jonsson and Lars Bergdahl,
The Effect of Wave Non-Linearity on the Forces on a Wind Turbine Foundation in Shallow Water,
In: Proceedings of EWEC 2003, European Wind Energy Conference & Exhibition, June 16 – 19, 2003, Madrid, Spain

Acknowledgement

This research has been carried out at the Department of Water Environment Transport, Chalmers University of Technology. The project was financially supported by the Swedish Energy Agency, which is gratefully acknowledged. The support from Åke and Greta Lisshed's foundation made the journey to the Offshore Mechanics and Arctic Engineering Conference and The European Wind Energy Conference possible and the foundation is also gratefully acknowledged.

I would like to thank my supervisor at the department, professor Lars Bergdahl, for his guidance in the world of water waves and for his swift answers to my questions. Further I would like to thank my supervisor, PhD Johan Jonsson at Volvo Technology Corporation, for valuable discussions and his never-ending optimism and support.

I would also like to thank my colleagues at the department for being encouraging and supportive. Both former and present PhD students in particular are appreciated for their friendship and for sharing their experience of being a PhD student. Jonas is especially mentioned for his help with questions about formalities, Endnote and Word.

I send my gratitude to my all my friends in the Chalmers Choir and in particular to Kerstin, Cecilia and Marie.

Thank you!

Göteborg, September 2003

Jenny Trumars

Contents

Abstract	i
Sammanfattning	iii
List of Appended Papers	v
Acknowledgement	vii
Contents	ix
Background	1
General Description of Wind Power Plants	2
Some Water Wave Fundamentals	3
Some Former Work on Random Non-Linear Waves	6
Some Former Work on Wave Action on Wind Power Plants	7
Test Site	8
Concept	11
SWAN	11
Realisation of Waves	13
Calculation of the Loads on the Structure	16
Implementation	17
Response	17
Results	18
Wave Transformation	18
Realisation	18
Conclusions and Discussion	25
SWAN	25
Realisations in the Time Domain	26
Forces	27
Further Work	28
References	29

Appended Papers: A and B

Background

The development of large wind power farms in the megawatt region has led to an establishment of wind power farms at sea. There are several reasons for this development: There are more suitable sites for wind power farms at sea than on land, where it can be difficult to find sparsely populated areas. The increase in energy produced from wind requires more space. Environmental disturbances as noise and negative visual impact can be removed from densely populated areas. Wind at sea has better quality; it is stronger and less gusty. On the other hand the placement at sea leads to new requirements on the structure, power grid and accessibility. For the support structure, in addition to standard loads, the wave load has to be taken into account and to calculate the wave load at the sites in question, theory for waves at finite depth has to be used.

For wind power off shore to be viable the aggregates have to be placed in relatively shallow water in depths ranging from 6 to 30 meters. At these depths the waves become non-linear due to the transformation as they travel from deep to shallow water. The non-linearities manifest as phase locking and wave breaking. The result is waves with higher sharper peaks and shallow troughs.

The scope of the thesis is to investigate an existing non-linear wave model for the calculation of wave loads on offshore wind energy converters. The purpose of the project as a whole is to contribute to knowledge about the load effect of waves on offshore wind energy converters and to facilitate suitable, efficient load models for fatigue and extremes.

General Description of Wind Power Plants

The wind energy converter consists of the turbine with its turbine blades, gearbox, generator and support structure. The energy producing part is the turbine converting the kinetic energy in the wind to electricity. To efficiently produce electric energy the turbine has to be placed at a level where the wind is strong and relatively unaffected by the ground or sea surface. For that purpose it is placed on a tower mounted on a foundation, making up the support structure of the wind turbine. Together the turbine, generator, gearbox and support structure are commonly called a wind energy converter. Different types of foundations for use off shore are the monopile, suction bucket, tripod or a gravity base foundation. The monopile is a circular tube piled or drilled into the soil and extending above the water surface, Figure 1. The tower is mounted directly on the monopile. This type of construction is used for the wind power farm at Bockstigen and the wave loads were calculated on that type of structure. The suction bucket is basically an upturned large bucket-like container inside which the pressure is lowered to make the structure stable and settle into the ground. A tripod is a lattice type of support structure see Figure 1. A gravity base foundation is kept in place solely by its weight see Figure 1 and can be made by *i.e.* a steel or concrete caisson which can be towed out to the construction site, be filled with ballast and sunk. Middelgrunden outside Copenhagen has gravity base support structures. To some extent these foundations can be combined with either a lattice type or a tubular tower. A more comprehensive introduction on wind power can be obtained at the Danish Wind Industry Association's home page www.windpower.org. (Danish Wind Industry Association - Danish Wind Energy Association, 2003)

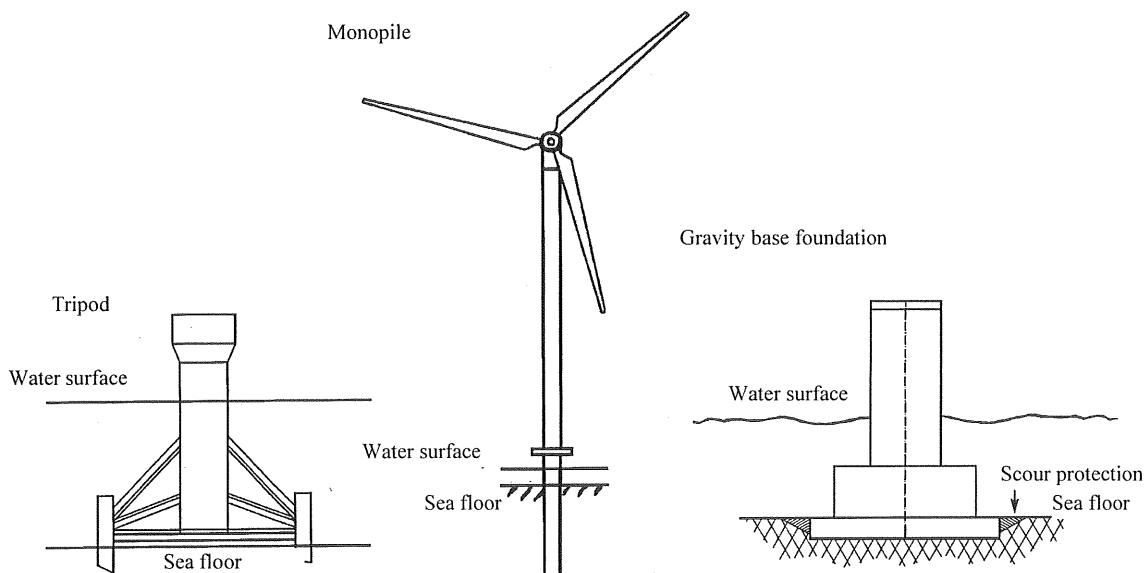


Figure 1. Different types of foundations for off shore wind energy converters.

Some Water Wave Fundamentals

The following is only a brief introduction to ocean waves and describes only a few of the issues at hand. To get a more complete description it is referred to literature on the subject. Some references are Massel (1996), Young (1999) and Mei (1983).

The properties of water surface waves are constantly changing depending on the environment around them. Wind is of vital importance, the resulting wind waves depend on the duration of the wind, the fetch and the wind speed. Loads from wind-generated waves are important for design purposes and there are several models describing the energy transfer from wind to waves *e.g.* Jeffreys' and Phillips-Miles models (Massel, 1996). When waves travel from deep sea towards land they transform due to the influence of bottom topography, bottom friction, wind and underlying currents. Changes in bottom topography cause effects like refraction, reflection, diffraction, and wave breaking. Diffraction is when waves are scattered by *e.g.* an obstacle. Refraction is when the propagation direction of the waves is changed by changing water depth. An example of refraction is that if the bottom has a gentle slope the waves get more and more parallel to the shoreline when they approach it. Refraction can cause focusing and spreading of the waves. Models simulating this transformation in the near shore region can be divided into phase-resolving and phase-averaging models. Using phase-averaging models the local statistical properties of the sea as *e.g.* the variation of directional variance spectra are modelled. Phase resolving models captures the deterministic properties of the sea *e.g.* the time- and space-varying sea surface elevation. The latter method captures the phenomena of troughs becoming shallower and peaks sharper, which are typical non-linear features of high waves at finite depth. On the other hand, by using short-term statistical properties from a phase-averaging model, a local realisation in the time domain can be obtained. However, it is vital that such a realisation retains the statistical properties of the sea state while reproducing the non-linear features. If non-linearities are of interest, a higher order realisation, *e.g.* using a higher order perturbation theory, has to be used.

Some basic definitions for a plane wave are illustrated in Figure 2. The free surface elevation $\eta(t,x)$ describes the surface of the water in time and space. The wave height H is the distance from peak to trough. For sinusoidal waves the amplitude is half the wave height but for irregular waves the wave height can be divided into positive and negative amplitudes, the positive amplitude a^+ is measured upwards from the still water level (SWL) and the negative a^- downwards. The wave period T is the time between two down or up crossings of the SWL and the wavelength L is the corresponding length. In the coordinate system the z-axis is defined positive upwards with the origin at the SWL and the x-y-plane coinciding with the still water surface see Figure 2.

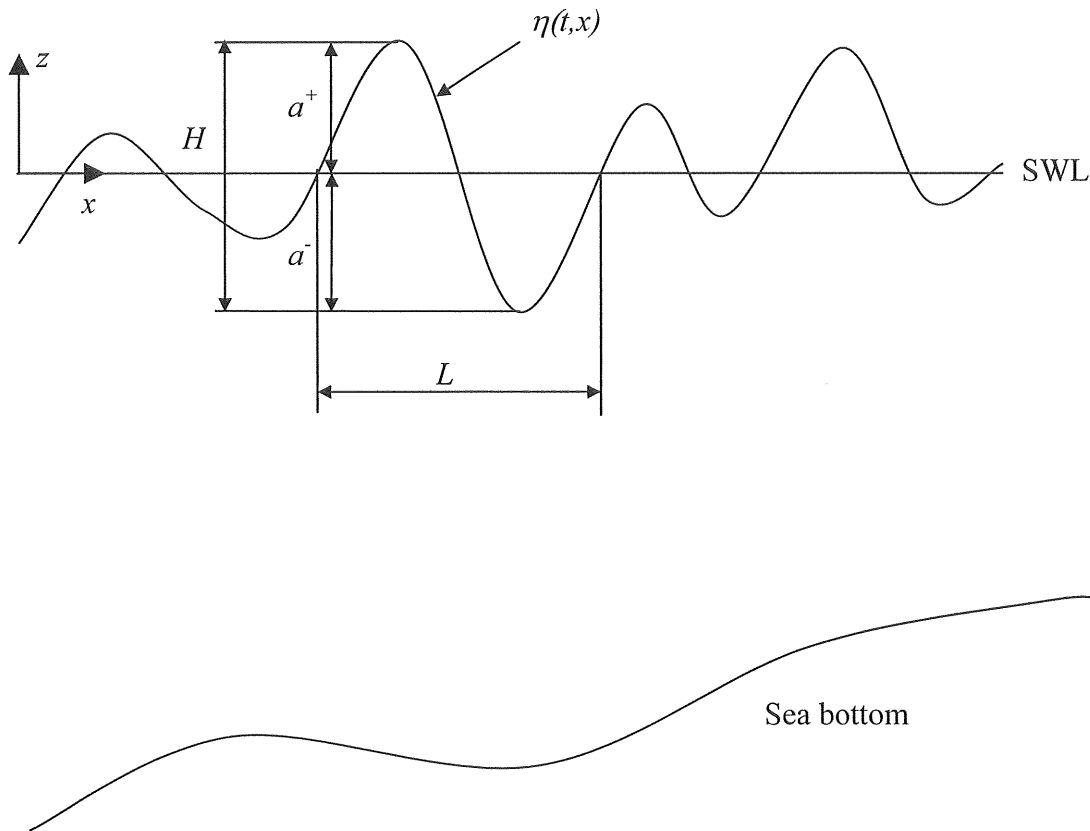


Figure 2. Basic definitions of a water wave in space.

The wavelength L and the wave period T are related through the dispersion relation,

$$\omega^2 = gk \tanh(kh) \quad \text{Equation 1}$$

where $\omega = 2\pi/T$ is the angular frequency and $k = 2\pi/L$ is the wave number. g is the acceleration of gravity and h is the water depth.

One of the simplest waveforms is that of a sine curve describing regular periodic waves. The surface of the sea, however, is more complex and often consists of irregular short crested waves. In such a case it is convenient to describe the sea surface in short-term statistics *e.g.* significant wave height, the mean of the one-third highest waves, energy content and variance content per frequency. The irregular wave surface can be synthesised by adding sinusoidal waves travelling in different directions. By choosing the appropriate properties, amplitude, phase angle and direction, of the individual waves the synthesised irregular wave surface can be given desired statistical properties. The frequency distribution of the variance, which can be described by a variance density spectrum where the variance at different frequencies is plotted, can describe a sea state

see Figure 3. The variance of the sea surface can be multiplied by a factor to give the local energy content of the waves and consequently the variance density spectrum is sometimes called energy spectrum. Some standard spectra are the JONSWAP and PM-spectrum (Faltinsen, 1990).

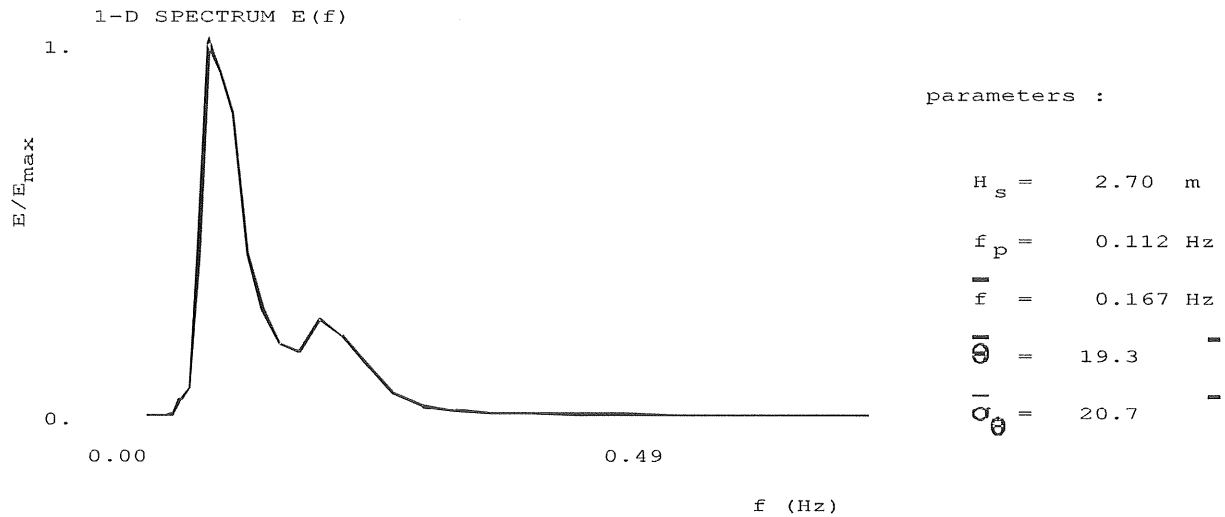


Figure 3. One-dimensional variance density spectrum.

To describe the variance of a directional sea where the waves travels in different directions a two-dimensional spectrum can be used as illustrated in Figure 4.

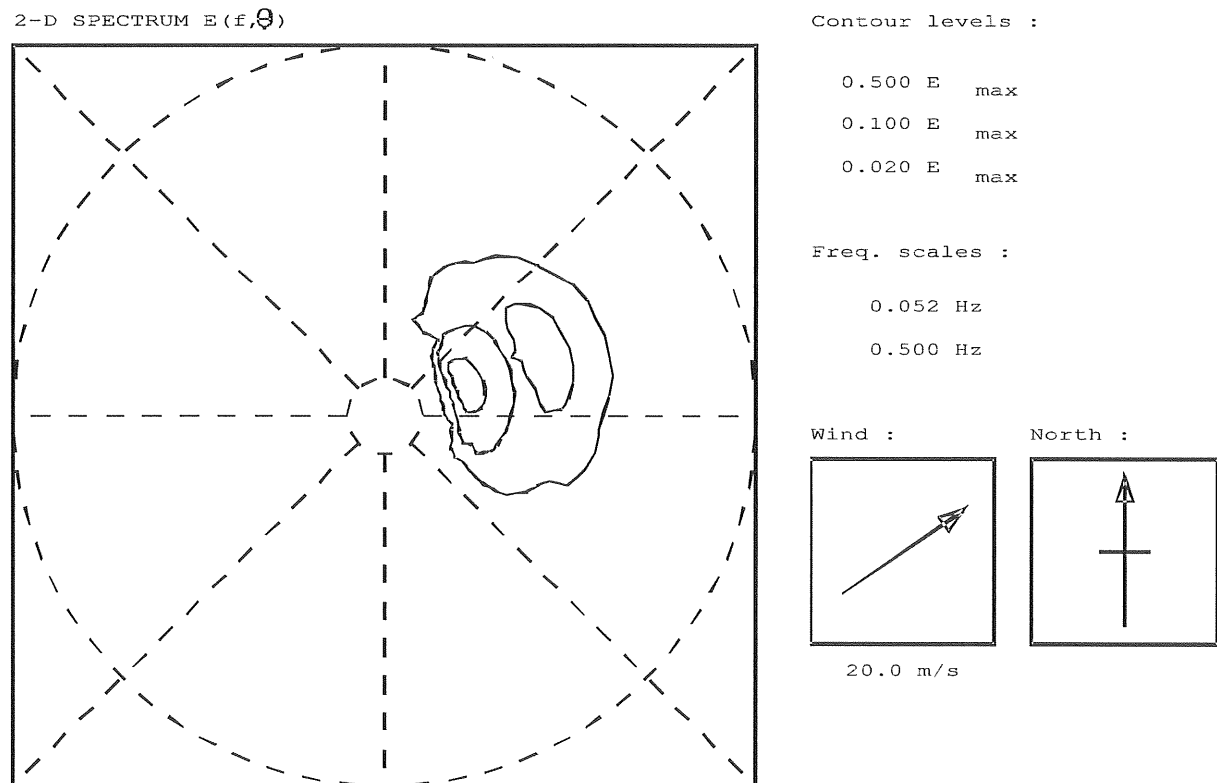


Figure 4. Two-dimensional variance density spectrum.

Variance density spectra can be used as input to the summation or synthetisation of waves mentioned above. The principle of the summation of component waves is shown in Figure 5 where the summation is done for the sea surface elevation.

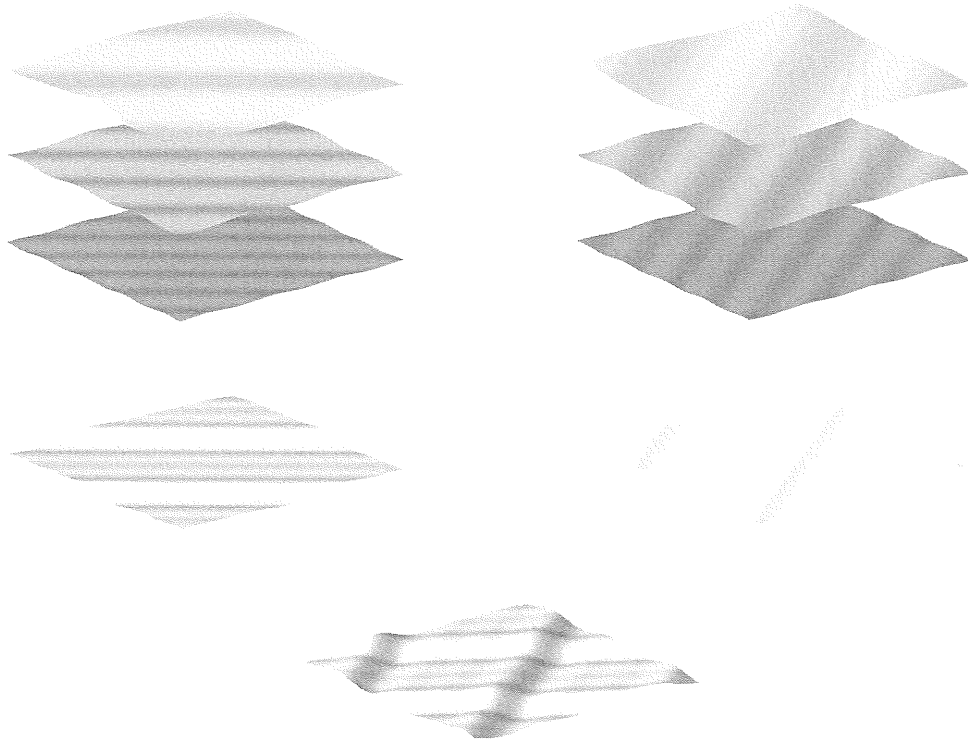


Figure 5. Principle of the summation of waves to yield an irregular sea surface.

The summation can be done over other properties than the sea surface elevation as e.g. the velocity potential of the fluid.

Some Former Work on Random Non-Linear Waves

Machado (2002) studies statistic analysis of non-gaussian environmental loads applied to non-linear waves and structure response. Machado formulates the equations for the realisation of non-linear waves according to Hasselmann (1962) and Hudspeth and Chen (1979).

Hudspeth and Chen (1979) formulate a method for the realisation, based on a spectrum, of waves in finite depth. The simulation is based on perturbation theory according to Hasselmann (1962). They use the Fast Fourier Transform to reduce the calculation time. An increase in variance due to the simulation is noted.

Stansberg (1998) makes a non-linear realisation of deepwater waves. A limitation of the local wave steepness is implemented to avoid unrealistic values, by truncating the higher frequencies of the spectrum used as a base for the realisation. The skewness of the surface elevation is studied by taking the ratio of the maximum value of a^+ and H . For non-linear waves the value increases from a value of 0.5 for linear waves.

A realisation to the third order of non-linear deep-water waves has been made by Nestegård and Stokka (1995). For the realisation the contribution to the total elevation from the third order perturbation series is small. The resulting total wave elevation yields steeper waves than for a realisation to the second order. It is recommended to study the effects on the velocity potential.

A comparison of different wave models against experimental data obtained from measurements of the velocity profile and elevation by laser was made by Stansberg and Gudmestad (1996). The studied wave models were a linear, a non-linear to the second order and a hybrid wave model. The hybrid model is similar to the second order realisation but the interaction of the waves is handled in a more physically correct way.

Some Former Work on Wave Action on Wind Power Plants

The calculation of wave action on wind power plants is dependent on the environmental conditions, the choice of method for calculating the water particle kinematics and the load model. A number of scientists have studied wave loads on offshore wind power plants and some are quoted below.

A study of loads from random waves and wind loads has been done by Oscar and Paez (1988). They use a linear random realisation of waves with Pierson-Moskowitz' spectrum as input for fully developed seas and the JONSWAP spectrum for fetch limited seas. The linear realisation is equivalent to the one used today for design purposes for random waves (Kühn, 2001). It is also used in Paper A and B for comparison with the higher order realisation.

For the European Wind Energy Conference in Copenhagen 2001 Henderson and Camp made a survey of the calculation of wave forces. They treat extreme load cases based on non-linear wave theory, stochastic calculation by linear wave theories, and they also bring up the subject of massive versus slender structures. (Henderson and Camp, 2001)

Sinclair (1994) studies the importance of aerodynamic damping on an offshore wind turbine. For calculation of the wave load linear wave theory and Morison's equation are used. He concludes that the aerodynamic damping is of vital importance for the behaviour of the structure.

In his PhD thesis Kühn (2001) deals with the entire design of an offshore wind power farm. For the analysis of irregular waves he uses linear theory and extreme waves are described by a higher order stream function theory. When calculating the velocities in the irregular linear waves to the instantaneous free water surface he uses Wheeler stretching,

that is the instantaneous velocity profile from bottom to the still water level is stretched from bottom to the instantaneous free surface. He concludes that for extreme waves non-linear wave models have to be used.

Cheng and van Bussel (2000) present a stochastic simulation of the structure and Cheng studies extreme response of wind power plants in his PhD thesis (Cheng, 2002). For the calculation of irregular waves he uses linear theory and for the calculation of extreme waves he uses regular non-linear waves. He applies Morison's equation without Wheeler stretching. In a more recent publication (Cheng and Henderson 2003) non-linear wave models for calculation of wave-loads on wind power plants are compared to measurements. However it is obvious that the used wave models do not correctly describe the wave elevation. The wave measurements are from Blyth and they clearly show non-linear features, the troughs being flatter and the peaks sharper.

Rogers (1998) uses stream function theory to the 11th order for non-linear regular waves and Morison's equation for the calculation of the forces. He concludes that the structural response is sensitive to alterations in soil stiffness, damping and wave period. He also discusses breaking waves and ringing.

van der Tempel and Molenaar (2002) treat the dynamics of the wind power plant in relation to the blade passing frequency and the frequency content in the waves. They discuss different design strategies to avoid overlap in the frequency content of the load and the eigenfrequency of the structure. Control of the turbine rotation provides means for avoiding overlap with the eigenfrequency. The aerodynamic damping and the soil properties play a vital part in the dynamics of the wind power plant.

Test Site

A first application of the thesis concept has been done at Bockstigen off the coast of Gotland in the Baltic Sea. See Figure 6 and Figure 7. The wind farm consists of five turbines of which one is instrumented for measurement of the structural response of the support structure. The wind and waves in the vicinity of the turbines are also measured. The bottom topography is obtained from sea charts of the area but more detailed bottom topography would be desirable.



Figure 6. The Baltic Proper with the location of Bockstigen marked with an arrow.



Figure 7. A detailed close-up at the location of Bockstigen off the coast of Gotland.

The wave climate in the Baltic Sea was studied during 1978 to 1982 by SSPA and spectra have been derived for those measurements. To illustrate the concept, in this study a spectrum for a wind speed of 20 m/s and open sea, at Ölands Södra Grund (Figure 6) was chosen as input to the SWAN model. The dominant wind direction is from the South West, which is in line with the longest fetch. (Wahl, 1983)

The bottom topography of the surrounding sea floor near the site was obtained from sea charts of the area. (Sjöfartsverket, 1979) The topography and the location of the wind farm can be seen in Figure 8.

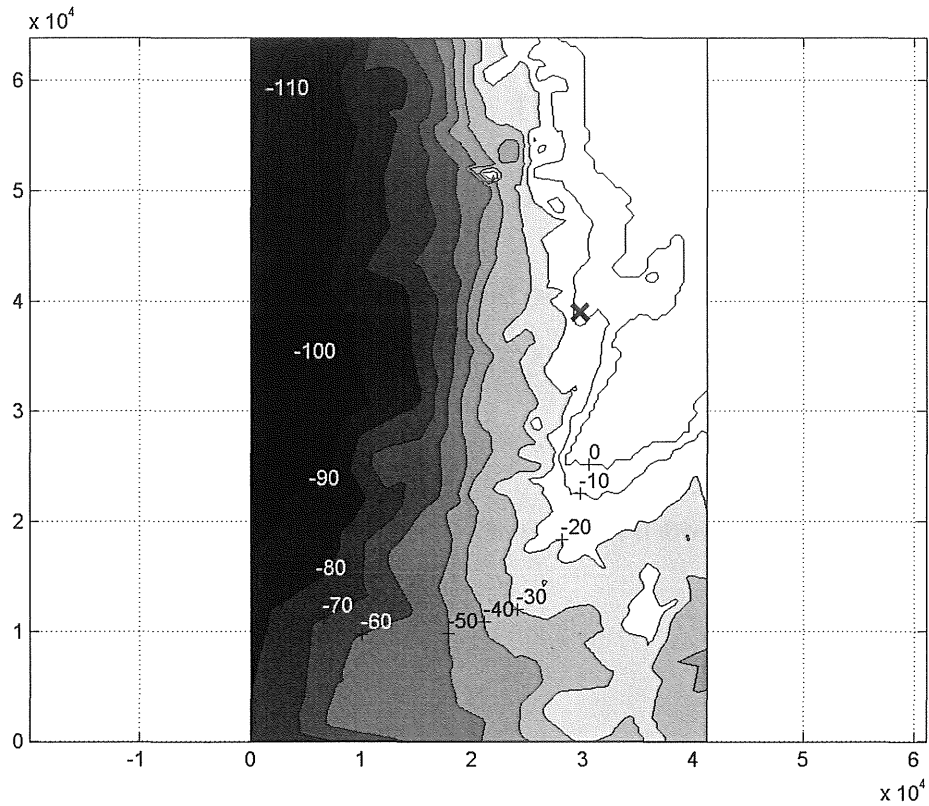


Figure 8. Bottom topography in meters of the surrounding ocean floor. The location of the wind farm is marked with X and the white colour is land. The scale on the axis is in meters.

The support structure of the wind turbine is a tower mounted on a cylindrical steel monopile drilled into the limestone and extending above the water surface. The cylinder diameter is 2.1 m and the mean-water depth is 6.5 m at the site. See Figure 9.

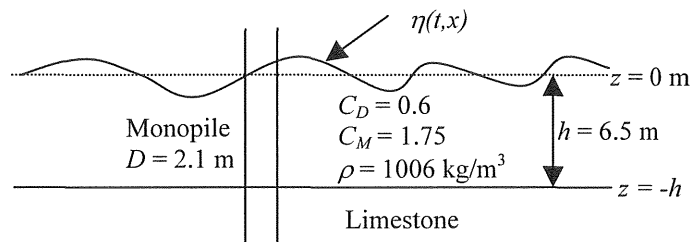


Figure 9. Details of the monopile. The monopile extends above the sea surface and the water depth is 6.5 meters. η is the instantaneous free water surface and the dotted line is the still water level.

An evaluation of the loads on the instrumented turbine has been made by Ronsten *et al* 2000 and they also thoroughly describe the instrumentation and the location of the wind farm. (Ronsten *et al.*, 2000) Since then a wave gauge has been added to the instrumentation. Evaluation of the wave measurements remains to be done.

Concept

For the present project SWAN (Simulating WAVes Near Shore) was chosen to model the wave transformation from deep sea to the near shore site of a wind farm. The result at the site is a wave spectrum describing the statistical properties of the waves by a variance density spectrum. These properties are used as input to a realisation of waves in the time domain. The loads on the structure are calculated with Morison's equation.

The flow of calculation is shown in Figure 10. The focus so far has been on the non-linear realisation, from short-term statistics, of waves in the time domain.

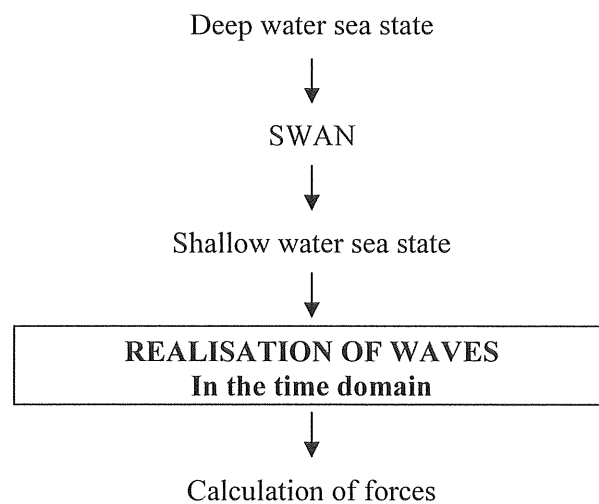


Figure 10. Chart describing the flow of calculation in the chosen concept.

SWAN

Swan is a phase averaging model developed at Delft University in the Netherlands. The transformation of the variance density spectrum from deep to shallow water is computed by an implementation of a transport equation modelling the transportation, production and dissipation of the properties of the waves. This is done by a finite difference scheme with source and sink terms. The difference between the different generations of wave models is how the source and sink terms are formulated. The first generation of wave models are based on empirical descriptions of the input to waves from wind and of the dissipation. The non-linear wave-wave interaction is absent in the first generation models. In the second generation of models the wind input is based on measurements of the normal stress exerted by the wind on the sea surface. A parametric representation of the quadruplet non-linear interaction is used (interaction within a group of four waves). For the third generation of models, including SWAN, the focus for improvement was on

the quadruplet interaction formulation and an approximation to the Boltzmann integral is used (DIA).

The Discrete Interaction Approximation (DIA) is an approximation to Boltzmann's integral describing interaction in sets of four waves. DIA limits the interactions to the most dominant ones. Due to the approximation the directional spread is larger than for models accounting for all interactions within the set of four waves. The approximation is not valid for unidirectional waves. Another limitation of the approximation, which SWAN has in common with all third generation wave models, is that it is also dependent on the frequency resolution. In SWAN an approximation of the non-linear interaction between three waves including only the most dominant interactions is used (The Lumped Triad Approximation, LTA). The approximation depends on the directional distribution of the wave spectrum. A description of phase averaging models can be found in e.g. Young (1999) and Massel (1996). A description of SWAN can be found in Holthuijsen *et al.* (2000).

Processes describing the propagation of waves available in SWAN are:

- Recti-linear propagation in space
- Refraction due to spatial variations in bottom topography and currents
- Shoaling due to spatial variations in bottom topography and currents
- Blocking and reflections due to opposing currents
- Transmission through, blockage by or reflection by sub-grid obstacles

Processes describing the generation and dissipation of waves available in SWAN are:

- Generation by wind
- Dissipation due to white-capping
- Dissipation by depth induced wave breaking
- Dissipation by bottom friction
- Wave-wave interactions (quadruplets and triads)
- Obstacles

Limitations of SWAN: Diffraction is not modelled and because of this SWAN should not be used where variations in wave height is large within a horizontal scale of a few wavelengths. Due to this the accuracy near large obstacles or in harbours is low. Wave induced currents are not calculated, however currents can be specified by the user as input. Wave induced set-up can be calculated.

The computational grid in SWAN covers an area of 41 240 m (x-axis) times 63 917 m (y-axis) and is divided in 100 times 150 cells. At the south and west border a two-dimensional JONSWAP spectrum is set as boundary condition. At the other boundaries the input is set to zero. The defining parameters for the JONSWAP spectrum are: peak enhancement factor 3.3; significant wave height 4.52 m; the peak period 6.72 s; the main wind direction is from the south west; the wind velocity at 10 m is 20 m/s and the directional spread is defined by a $\cos^2(\theta)$ function. The computational domain and the underlying bottom topography are depicted in Figure 8.

Realisation of Waves

The realisation of waves in the time domain is based on work by Hasselmann (1962) and Hudspeth and Chen (1979) and the equations are presented in Paper A and B. The spectrum obtained at the site of the wind power plant is used as input to the realisation. The time series is calculated as a Fourier sum of sinusoidal wave components. Both the elevation of the sea surface and the velocity potential is calculated. This is done to a first order approximation and to a second order approximation. The velocity is then extrapolated, for both the first and second-order realisation, to the instantaneous free water surface by a first order Taylor expansion. The solution to the first order expansion is commonly used to describe the properties of irregular waves in the time domain.

An approximate solution to the boundary value problem of free surface waves can be obtained by a perturbation expansion of the velocity potential Φ and the water surface elevation η in perturbation series (Hasselmann, 1962). The constraint is that the wave height to wavelength ratio must be kept small. The resulting expressions, to the second-order perturbation equations, are presented in Paper A (Hudspeth and Chen, 1979; Machado, 2002). The solutions to the perturbation equations are expressed as Fourier series. The boundary conditions and an example of the solution of the perturbation equations for the surface elevation are given below.

The boundary value problem for the irrotational flow of surface gravity waves in an incompressible, homogeneous and inviscid fluid can be expressed in terms of a velocity potential $\Phi(x,z,t)$. The water particle velocities are given by the spatial derivative of Φ as

$$u = -\Phi_x \quad \text{Equation 2}$$

$$w = -\Phi_z \quad \text{Equation 3}$$

where the subscript denotes partial differentiation.

The coordinate system is chosen so that the positive, vertical z-axis is pointing upwards and the x-axis is in line with the still water surface at $z = 0$. The governing differential equation is the Laplace equation, which is given in Figure 11 together with the boundary conditions at the sea bottom and the free surface. The sea bottom is assumed to be locally horizontal and flat which conforms to mild slope conditions.

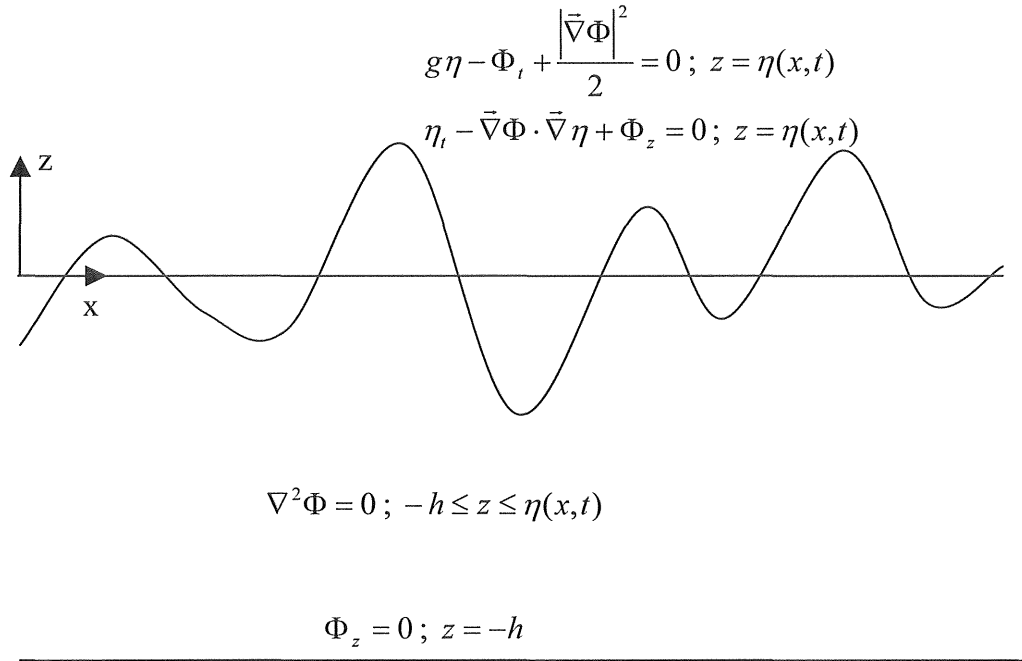


Figure 11. Boundary conditions and governing differential equation for the irrotational flow of surface gravity waves.

An example of the method with perturbation series and the solution for the first- and second-order contributions to the surface elevation is given below.

The perturbation expansions for the free surface elevation η can, for small waves, be expressed as

$$\eta(x, t) = \sum_{j=1}^{\infty} \eta_j(x, t) \quad \text{for} \quad t > 0 \quad \text{Equation 4}$$

where j denotes the perturbation ordering parameter.

The solution to the linear problem and the first order contribution can be expressed by the Fourier series

$$\eta_1(x, t) = \sum_{m=0}^N F(m) \exp i(\omega_m t - k_m x), \quad \text{Equation 5}$$

where the wave number k is given by the dispersion relation

$$\omega_m^2 = gk_m \tanh k_m h, \quad \text{Equation 6}$$

i is the imaginary unit, ω is the angular frequency, g is the acceleration of gravity and h is the water depth.

The solution to the second-order contribution becomes

$${}_2\eta(x,t) = \sum_{n=0}^N \sum_{m=0}^N \frac{F(n)F(m)}{2g} H(\omega_n, \omega_m) \exp i[(\omega_n + \omega_m)t - (k_n + k_m)x], \quad \text{Equation 7}$$

where

$$H(\omega_n, \omega_m) = 2(\omega_n + \omega_m)D(\omega_n, \omega_m) - \frac{g^2 k_n k_m}{\omega_n \omega_m} + (\omega_n + \omega_m)^2 - \omega_n \omega_m \quad \text{Equation 8}$$

and

$$D(\omega_n, \omega_m) = \frac{2(\omega_n + \omega_m) \left[g^2 k_n k_m - (\omega_n \omega_m)^2 \right] - \omega_n \omega_m (\omega_n^3 + \omega_m^3) + g^2 (\omega_m k_n^2 + \omega_n k_m^2)}{2\omega_n \omega_m \left[(\omega_n + \omega_m)^2 - g(k_n + k_m) \tanh(k_n + k_m)h \right]}. \quad \text{Equation 9}$$

The complex amplitude $F(n)$ is given by

$$F(n) = \sqrt{2S(\omega_n)\Delta\omega} \exp(-i\varepsilon_n) \quad \text{Equation 10}$$

where S is the variance density spectrum, $\Delta\omega$ is the frequency resolution and ε a random phase angle distributed between 0 and 2π .

Equations 4 through 10 are valid for finite depth and small waves (Hasselmann, 1962; Hudspeth and Chen, 1979; Machado, 2002).

The solution to the second order perturbation equations is more complex and the phases of the components in the Fourier sum are no longer free but are locked to the first order wave components. Variance is added to the higher frequencies. The results from the first and second order realisation are added to form the total elevation according to Equation 4, see Figure 12.

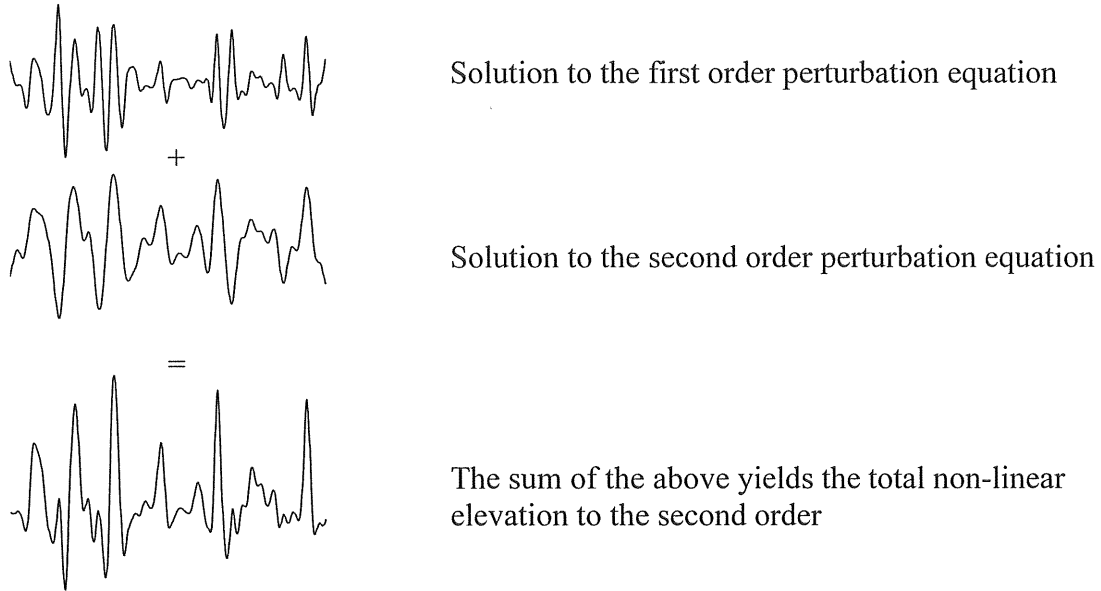


Figure 12. The results from the first and second order realisation are added to form the total elevation according to Equation 4.

The same method of summation is applied for the velocity potential. The wave particle velocities are obtained from the spatial derivative of the velocity potential and the acceleration from the time derivative of the velocity. In order to prevent the calculated velocities above the still water level from becoming unrealistically high, an approximation to the wave particle kinematics is implemented by a Taylor expansion to the first order around $z = 0$ (Nestegård and Stokka, 1995). This approximation is used for both the linear and non-linear realisation.

Calculation of the Loads on the Structure

The force on the structure is calculated with Morison's equation to the instantaneous free water surface. The coefficients in Morison's equation are based on experimental work and they depend on the cross-sectional shape of the structure. They also depend on the frequency content of the waves. The restriction on Morison's equation is that the wavelength to structure diameter ratio has to be small $\lambda > 5D$ (Faltinsen, 1990).

The wave forces P and resulting base moment M on the monopile are calculated by using Morison's equation integrating from the bottom to the instantaneous free surface

$$P = \frac{1}{2} \rho C_D D \int_{-h}^{\eta} u |u| dz + \rho \frac{\pi D^2}{4} C_M \int_{-h}^{\eta} u_t dz \quad \text{Equation 11}$$

and

$$M = \frac{1}{2} \rho C_D D \int_{-h}^{\eta} u |u| (z+h) dz + \rho \frac{\pi D^2}{4} C_M \int_{-h}^{\eta} u_i (z+h) dz . \quad \text{Equation 12}$$

Where C_D is the drag coefficient, C_M is the inertia coefficient, ρ is the water density and D is the diameter of the monopile. See e.g. (Faltinsen, 1990). The coefficients and other constants are given in Figure 9.

Implementation

This concept has been implemented in the two papers in appendix A and B. In A the simulation is done with an ordinary Fourier sum over all components. The process is slow and a limited number of short simulations were done. In paper B the realisation was made by means of an Inverse Fast Fourier Transform and ten realisations over one hour were made. The higher order realisation produces unrealistically high waves exceeding the wave-breaking limit of $0.78 h$ and results above this limit have been discarded in paper A. In paper B this procedure was not possible due to the longer realisations instead an excerpt of a period with waves below the wave-breaking limit is shown. The main focus was then to study the effects on the energy or variance content of the non-linear realisation compared to the linear realisation. In order to do so variance density spectra were calculated for both the linear and non-linear realisations.

The frequency resolution for the simulation using the FFT is $1.65 \cdot 10^{-3}$ rad/s and the time resolution is 0.5 s. For the ordinary summation the resolutions are $1.5 \cdot 10^{-2}$ rad/s and 0.13 s for frequency and time domain respectively.

Response

When designing the support structure the response is vital. It is not certain that the largest waves create the most damaging response. If the frequency of the load coincides with the eigenfrequency of the structure resonant behaviour may occur. The initial calculation of the wave load is made on a rigid structure. When calculating the structural response simulation of the elastic structure, the soil structure interaction and the aerodynamic damping from the turbine is of importance. (Kühn, 2001; Sinclair, 1994)

The control of the turbine itself is also a factor of interest; it can be run in a manner to avoid certain frequencies. This has been studied by van der Tempel and Molenaar (2002) who also address the problem with the rotor and blade passing frequency. The blade passing frequency should not overlap the natural frequency of the support structure. When a variable speed turbine is used the rotor and blade passing frequency covers a larger range. In such cases the control of the turbine can be used to avoid operating it at the eigenfrequency of the structure. Such an approach is used at Utgrunden in Sweden. Notable is also that when designing a soft support structure, with a natural frequency below the rotor frequency it is likely to enter the frequency domain of the waves. (Kühn, 2001; van der Tempel and Molenaar, 2002)

Results

Wave Transformation

The results obtained from SWAN are e.g. variance density spectrum and significant wave height. A plot of the geographical distribution of the calculated significant wave height near the site of the wind power plant can be seen in Figure 13.

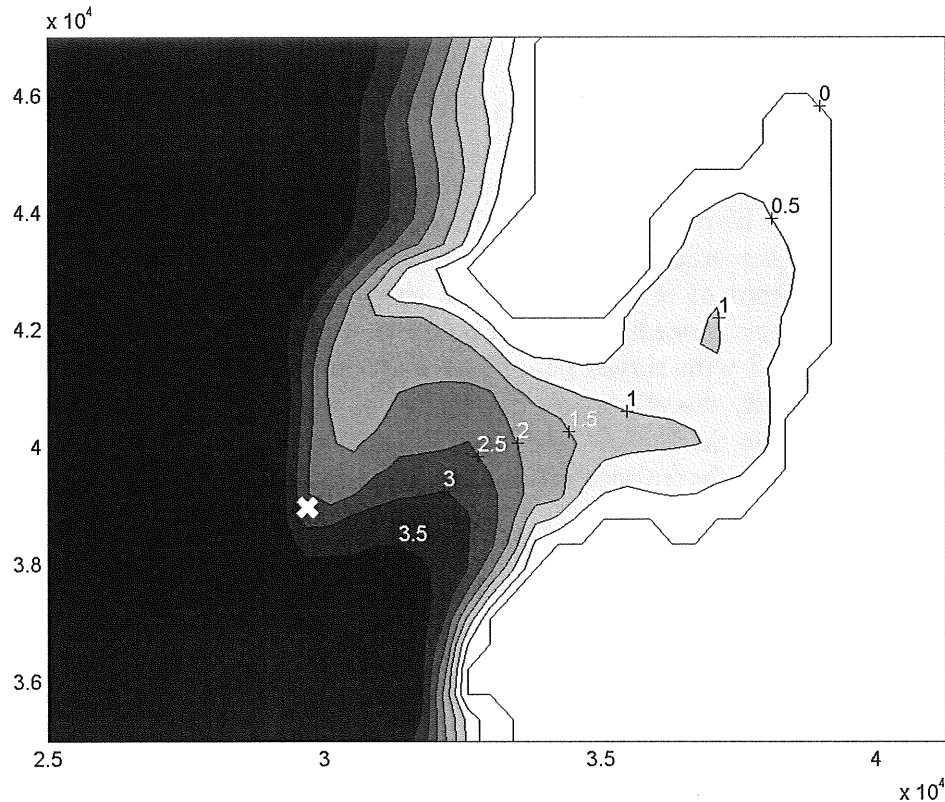


Figure 13. Significant wave height in meters. The location of the wind farm is marked with X and the white colour is land. The scale on the axis is in meters.

Realisation

The loads on the structure increases, compared to the linear model, when using the non-linear realisation. If the wave height is kept below the wave-breaking limit, paper A, the results seem realistic. But if the realisation is done without restrictions on the wave height, paper B, the waves become clearly unrealistic and consequently so does the wave load. In paper B ten realisations over one hour were carried out and a spectral analysis of the results was made. In paper A the realisation was made over a shorter period and cannot be used as a basis for frequency analysis. In both papers the skewness of the load increases partly because of the use of Morison's equation but also due to the fact that there is a change in the water particle kinematics. See Table 1.

In paper A the realisation was made over a time of 63 seconds and the sea surface elevation, force and base moment from both the linear and non-linear realisation have been calculated throughout that time period.

Figure 14 shows the total non-linear sea surface elevation and the first and second-order contributions to it. At the end of the realised time history, $t = 60$ s, the wave takes the ideal form and the trough before the peak has become more shallow compared to the first-order simulation and the peak is sharper. The result at $t = 20$ s shows an overshoot of the second-order contribution resulting in a trough below the first-order realisation. This could indicate that the simulated waves are violating the small amplitude requirement.

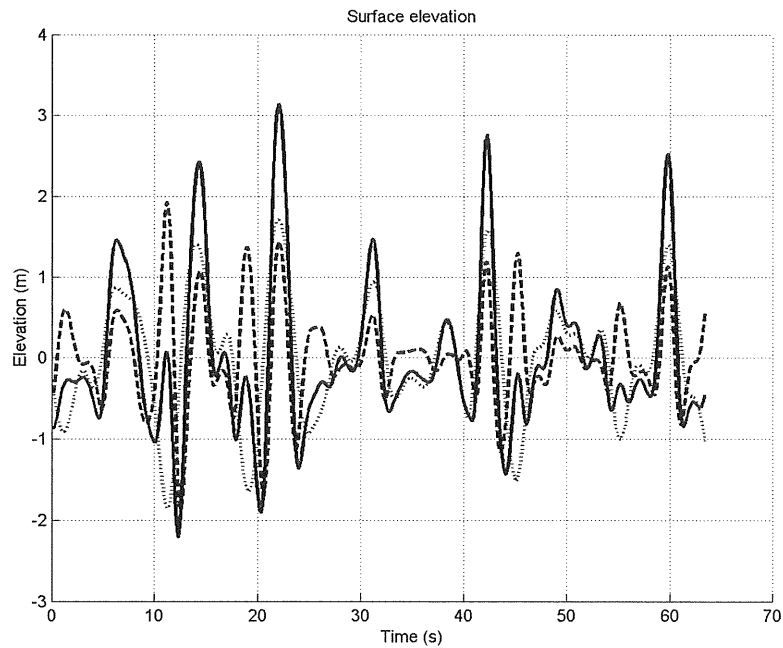


Figure 14. Surface elevation in meters. The solid line represents the total non-linear elevation, the dotted line shows the first-order contribution and the dashed line shows the second-order contribution.

The forces and base moments are calculated according to Equation 11 and 12 throughout the time series. Figure 15 and Figure 16 shows the surface elevation compared to the depth integrated force and base moments for the first and second-order realisation respectively. The force is scaled down by 10^5 and the moment with 10^6 in order to get a clear picture of when they have a maximum or minimum compared with the sea surface elevation. The maximum force and base moment is at the zero up crossing of the highest wave. This indicates that the force is inertia dominated.

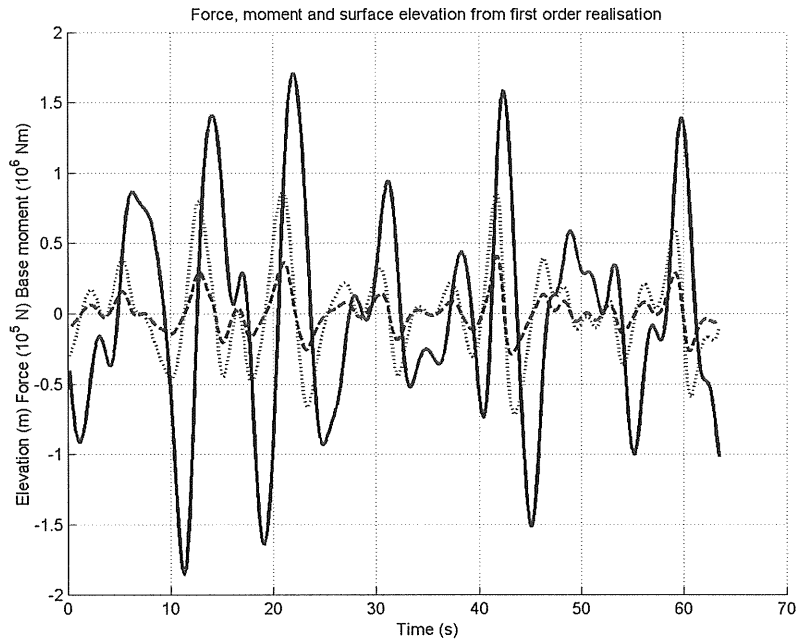


Figure 15. The surface elevation compared to the force and the base moments calculations from the first-order realisation. The solid line shows the total elevation (m), the dotted line shows the force (10^5 N) and the dashed line shows the base moment (10^6 Nm).

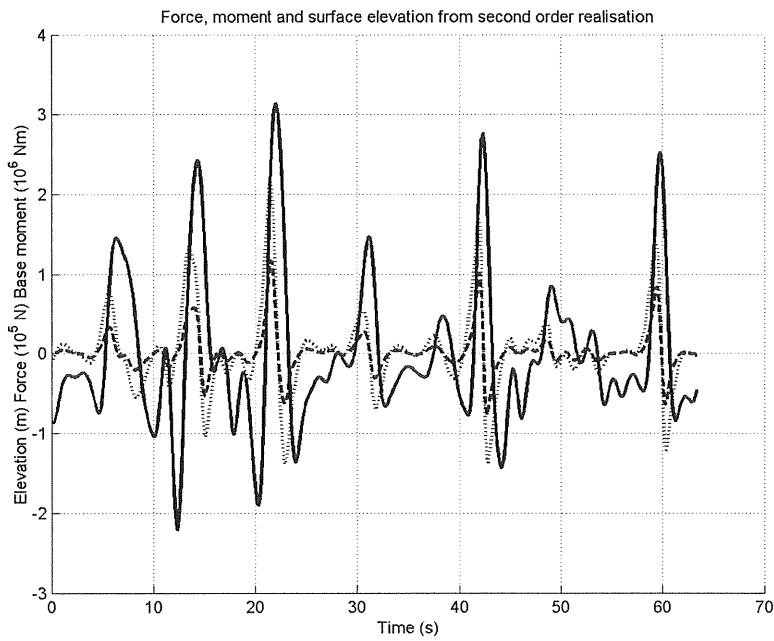


Figure 16. The surface elevation compared to the force and the base moments calculations from the second-order realization. The solid line shows the total elevation (m), the dotted line shows the force (10^5 N) and the dashed line shows the base moment (10^6 Nm).

From a comparison of the results from the first and second-order realisation it can be seen that the second-order realisation yields higher loads. This is mainly due to higher particle accelerations and to a minor degree on higher velocities and larger submergence in the second-order realisation.

For the comparison of the elevations the ratio a_{\max}^+/H_{\max} was studied where a_{\max}^+ is the positive amplitude for the maximum wave and H_{\max} is the corresponding wave height. When the troughs are becoming shallower and the peaks sharper for the second order realisation, showing asymmetry around the still water level, this ratio increases. This effect can also be studied in the force and the base moment, see Table 1. However, it is not as pronounced as for the elevation. When calculating the ratio for the force and base moment H_{\max} is the maximum trough to peak value and A_{\max} is the corresponding positive amplitude.

Table 1. The ratio a_{\max}^+/H_{\max}

Order of realisation	First	Second
Elevation	0.51	0.62
Force	0.57	0.61
Base moment	0.58	0.65

The force and base moment display asymmetry around zero also for the first-order realisation and it is increased further for the second-order realisation. In the first-order case the asymmetry is caused by the use of Morison's equation integrating from the bottom to the instantaneous free surface, Eq. 11 and 12, and the higher particle velocities at the crests of the waves.

For a large number of realisations over longer times the mean of the ratio for the first-order wave elevation will be 0.5.

When calculating forces distributed along the monopile focus is on the highest peak, at $t = 22$ s, of the surface elevation in Figure 14. Velocities and accelerations were calculated at half meter intervals starting from the sea bottom, $z = -6.5$ m. The results for the velocity are shown in Figure 17. The loading force was calculated in the middle of each interval. The times of the calculations were chosen around the highest peak. They coincide with the trough $t = 20.3$ s, zero up crossing $t = 21$ s, peak $t = 22$ s and zero down crossing $t = 23$ s of the surface elevation. Studying the distribution along the monopile, one finds that the highest local velocity is at the peak and the highest local acceleration and force is at the zero down and up crossings. See Paper A.

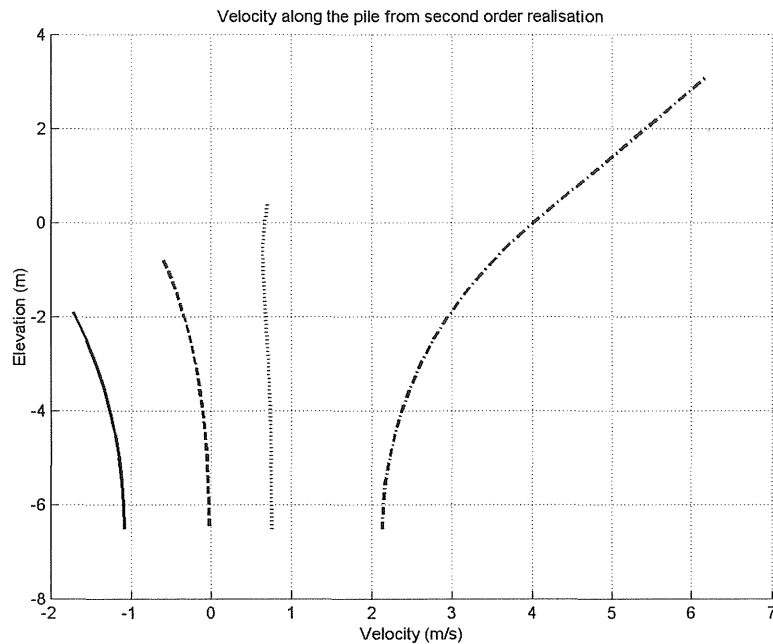


Figure 17. Velocity as a function of surface elevation. The solid line shows velocity at $t = 20.3$ s, the dashed line at $t = 21$ s, the dot dashed line at $t = 22$ s and the dotted line at $t = 23$ s.

In Paper B ten linear and non-linear realisations of one hour duration were made and the forces on the structure were calculated for all ten cases. Variance and power-spectra for elevation, force and base bending-moment were calculated from the obtained time-series. The mean and standard deviation for the spectra were calculated and the spectra were smoothed. For the linear time-series the standard deviation of the spectra is small. Computing the non-linear realisation of the waves there is an increase in the variance of the sea-surface elevation compared to the first-order linear case. Stansberg (1998) also get an increase when calculating non-linear deep-water waves but to a much lesser degree. The increase is due to the addition of higher frequency components in the non-linear realisations, as can be seen in Figure 19. The increase in variance produces unrealistically high waves, exceeding the wave-breaking limit of $0.78 h$ (CERC, 1977), which in this case is 5.07 meters. It can also be observed that the spectrum is broadbanded and produces ripples. See Figure 18. For waves below the wave-breaking limit the waves and the forces exhibit the desired non-linear effects of troughs becoming shallower and peaks sharper, Figure 18.

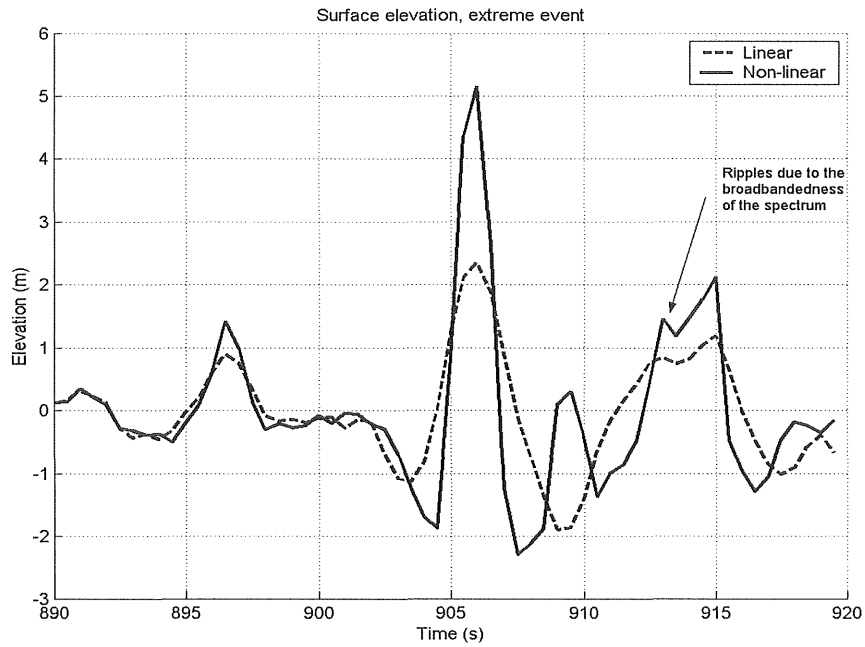


Figure 18. Non physical extreme wave above the wave-breaking limit of 5.07 meters

Power spectra were calculated for both the linear and non-linear realisations, from the entire one hour time series, in order to study the high-frequency contribution from the non-linear realisation.

The second-order contribution to the surface elevation is sensitive to the high frequency end of the linear input spectrum calculated in SWAN. The variation of the spectral density for the non-linear realisation is significant, Figure 20. For the linear case the variation is small.

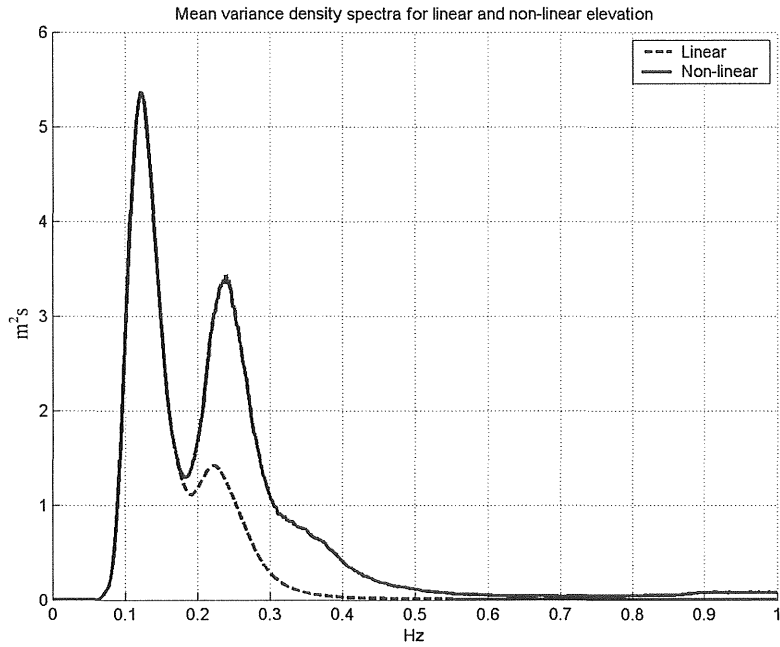


Figure 19. Mean variance density spectra for the linear and non-linear elevation.

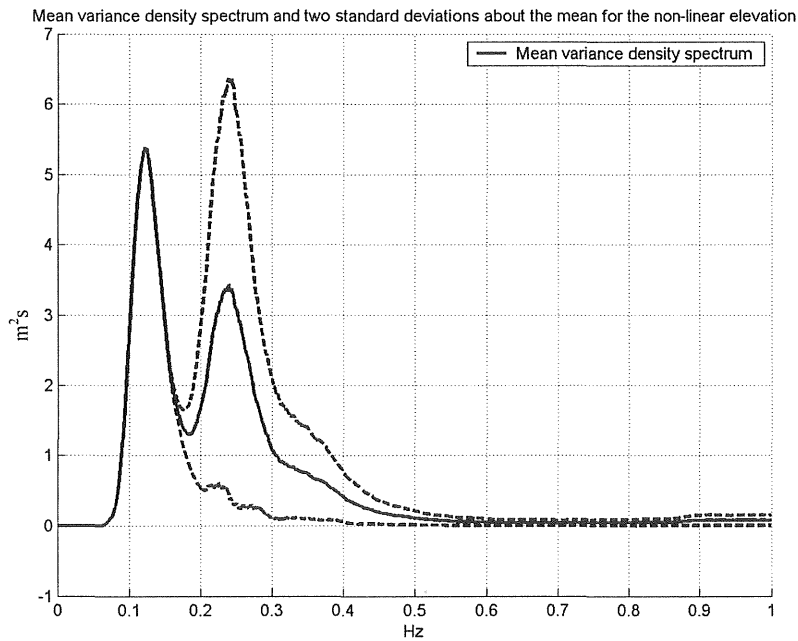


Figure 20. Mean variance density spectra and two standard deviations about the mean for the non-linear elevation.

The mean power spectra for the force and base moment are highly influenced by a time-series with a maximum wave height of 13 meters, Figure 21. The effect is enhanced by the use of Morison's equation where the velocity is squared. The variation in the results for the force and base moment is large, see Paper B. In Figure 21 the spectra for all the

time series of force are plotted and the one marked with an arrow is the one with the 13 meter maximum wave height.

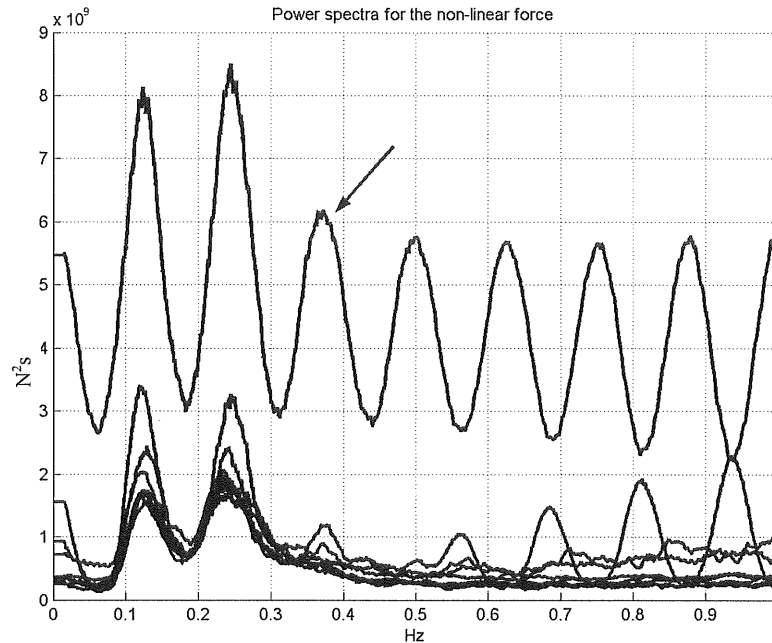


Figure 21. Power spectra for all ten time-series of the non-linear force. The spectrum marked with an arrow is from a time-series with a maximum wave of 13 meters.

For the base moment the influence from the time-series with the maximum wave height of 13 meters is even more pronounced. This is due to the lever ($z + h$) in Equation 12.

The variance of the time-series in Paper B increases from 0.43 m^2 to 0.69 m^2 for the water surface elevation, from $7.50 \cdot 10^8 \text{ N}^2$ to $6.58 \cdot 10^9 \text{ N}^2$ for the force and from $1.12 \cdot 10^{10} (\text{Nm})^2$ to $6.39 \cdot 10^{11} (\text{Nm})^2$ for the base moment.

Conclusions and Discussion

SWAN

So far the focus has been on the realisation of waves in the time domain from short-term statistics. Thus the emphasis has not been on the simulations carried out in SWAN. Another reason is that we wanted to wait for more results from the wave measurements. A matter of interest is then to check the results from SWAN with the measurements from Bockstigen. Other aspects are to check the grid independence of the solution, the size of the calculation domain and the sensitivity to variations in wind input. A sufficient accuracy of the wind input should not be a problem within the wind energy community; wind is after all the vital issue. The bottom topography in this study was obtained from sea-charts; it is better to use site-specific measurements since the data from sea-charts can be of varying quality and age.

Realisations in the Time Domain

It is observed that the calculated depth integrated forces and base moments, positive and negative, are highest close to the zero crossings of the surface elevation. This is due to the high water particle accelerations. It is also observed that the non-linear realisation gives larger maximum forces and base moments than the linear realisation due to the change in the kinematics of the water particles.

The described method provides a way of calculating non-linear irregular waves at finite depths. However, the chosen method for calculating non-linear waves produces unrealistically high waves if a restriction on the maximum wave height is not applied. In Paper A this problem was avoided by discarding realisations with a wave height above the wave-breaking limit of $0.78 h$ (5.07m). In Paper B this is not possible due to the longer time of the realisation. There were no realisations where the wave height was below 5.07m for the entire hour.

The use of $0.78 h$ as the wave-breaking limit can be conservative as the limiting value for H_{max} of $0.55 h$ is found to apply to shallow water waves. This is a more restrictive value than the breaker height limit $0.78 h$ for mildly shoaling bottoms used in the calculation above. The implication is that for shoaling cases $0.78 h$ should be used and for vast shallows $0.55 h$ may be more accurate but less conservative. A discussion on the largest wave height in water of constant depth can be found in Massel (1996).

A local wave steepness limiter according to Stansberg (1998) will take care of some part of the problem and will also reduce the broadbandness. A restriction based on keeping third-order omitted terms smaller than the corresponding second-order terms is enforced. This gives lower local wave steepness with associated velocities and accelerations, resulting in more physically correct forces. The local wave steepness limiter end in a restriction on the wave number and consequently on the angular frequency. The restriction can be implemented by a cut-off at the high-frequency end of the input spectrum.

A test of a frequency cut-off showed that it did reduce the broadbandness but had hardly any effect on the maximum wave height. Another way, which we have not tested, of reducing the wave height could be to use a standard spectrum, fitted to the first peak of the non-linear SWAN spectrum, for the realisation. After the realisation is carried out a spectrum from the time-series can be constructed to be compared with the near-to-shore SWAN spectrum. The motivation for using this method is that the theories used in SWAN for calculating the evolution of the non-linear spectrum and the way the non-linear realisation is performed are similar. As a result of this the non-linear contributions are added twice, first in SWAN and then in the second-order perturbation equations. Further the second-order contribution in the realisation is sensitive to the tail end of the linear input spectrum where the second peak is. This can further increase the variance at those frequencies for the second-order realisation.

As stated in Paper A the linear solution retains the variance of the input spectra, however one can claim that there should be a larger spread in the variance for finite wave records. To achieve this an appropriate variation can be added to the amplitudes obtained from the variance density spectra (Machado, 2002; Tucker *et al.*, 1984).

In the realisation using the FFT the frequency and time resolutions are interdependent. Therefore if a higher time resolution is required for a given frequency resolution the Nyquist frequency has to be moved to higher frequencies and this also brings about an increased number of components.

Implementing a Fast Fourier Transform (FFT) method has made the Fourier sums faster which allows for a larger number of simulations over longer time-periods and statistical analysis of the results. The limiting factor for the calculation is then the size of the matrix which forms the basis for the inverse FFT of the double sum required for the second-order contribution.

Forces

When calculating the forces Morison's equation was chosen which is motivated by the fact that the structure diameter is small compared to the wavelength, $L > 5D$, *i.e.* a hydrodynamic transparent structure which does not affect the wave motion. The coefficients in Morison's equation depend on the ratio between wavelength and structural diameter and on the ratio between the water particle excursions and structural diameter. The first dependence indicates that Morison's equation is less suitable for use in irregular waves. The latter dependence indicates that the coefficients should vary vertically along the monopile as the particle orbit diameter decrease with submergence. For shallow water waves the decrease is, however, marginal. One way to compensate for that could be to implement a panel method in an area close to the cylinder and use the realisation in the time domain at the border of that area. However, since the panel method is used for non-viscous irrotational flow at high Reynolds numbers this does not account for flow separation and vortex shedding and would give no drag force, which maybe the dominant force for slender structures. The next step would be to use a viscous model as for example a Reynolds Averaged Navier Stokes model but that would be very computationally demanding. From a practical engineering point of view Morison's equation is sufficient and the coefficients C_D and C_M can be adjusted to fit the conditions at hand. Biofouling increases the apparent diameter of the structure and changes the roughness, which gives other coefficients. A discussion on Morison's equation can be found in Faltinsen (1990).

When the realisation is made without the restriction in wave height in Paper B the effect on the force and base moments is very large as a result of using Morison's equation where the effect from increased velocitys and accelerations enters and is further amplified by the coefficients the integration along the monopile. See Equation 11 and 12.

The choice of load model is discussed in Kühn (2001). For structures that are not hydrodynamically transparent the wave-diffraction effects the force and has to be taken into account by for example a panel method.

Further Work

Validation of the wave and load calculations will be carried out within the measurement program at Bockstigen. The loading on the structure has to be derived from the measured internal load effects (structural shear forces and moments), and consequently the flexibility of the structure has then to be considered.

The accuracy in SWAN should be checked by comparing wave spectra from the measurements at Bockstigen with spectra calculated in SWAN for some weather conditions.

The problem with the high increase in variance and the unrealistically high waves has to be addressed and a first step is testing the approach of using a standard spectrum fitted to the first peak in the non-linear SWAN spectrum and see if the non-linear contribution from the second-order realisation is of the same magnitude as the second peak in the transformed SWAN spectra.

Make a model of the structure where the elastic behaviour of the structure itself and of the soil properties is implemented. The response of the simulated and the real structure can then be studied by multivariate analysis to see whether the load model induces the same dominant features of the response as is measured.

The model of the structure can be used to investigate the need for a fluid structure interaction and to what degree the interaction has to be implemented. The relative motion of the structure can be added in Morison's equation.

There is a large amount of data available from the measurement program at Bockstigen and before proceeding with the development of the load model it is of interests to study the data and investigate which loads dominate the response of the structure.

References

- CERC. (1977). *Shore Protection Manual* (Vol. 1). Fort Belvoir: U.S Army Coastal Engineering Research Center
- Cheng, P. W. (2002). *A Reliability Based Design Methodology for Extreme Responses of Offshore Wind Turbines*. Dept. of Wind Energy Research Institute, Delft University, Delft
- Cheng, P. W. and Henderson, A.R. (2003). Non-linear Random Wave Loads on Support Structures of Offshore Wind Turbines. In: *Proceedings of the European Seminar Offshore Wind Energy in Mediterranean and Other European Seas, April 10-12 2003*, (pp. 239-253). Naples, Campania, Italy.
- Cheng, P. W. and van Bussel, G. J. W. (2000). Assessment of combined extreme load conditions for offshore wind energy converters. In: *Proceedings of the 10th International Offshore and Polar Engineering Conference, May 28-Jun 2 2000*, (pp. 492-498). Seattle, WA, USA.
- Danish Wind Industry Association - Danish Wind Energy Association. (2003). <http://www.windpower.org/>. [World Wide Web]. Danish Wind Industry Association - Danish Wind Energy Association. [2003, Sep 9].
- Faltinsen, O. M. (1990). *Sea loads on ships and offshore structures*. New York: The Press Syndicate of the University of Cambridge. 0 521 45870 6
- Hasselmann, K. (1962). On the non-linear energy transfer in a gravity-wave spectrum Part 1. General theory. *Fluid Mechanics*, **12**
- Henderson, A. R. and Camp, T. R. (2001). Hydrodynamic Loading of Offshore Wind Turbines. In: *Proceedings of the European Wind Energy Conference*, Copenhagen, 2-6 July.
- Holthuijsen, L. H., Booij, N., Ris, R. C., Haagsma, I. G., Kieftenburg, A. T. M. M. and Kriezi, E. E. (2000). User Manual, SWAN Cycle III version 40.11. Delft: Delft University of Technology.
- Hudspeth, R. T. and Chen, M.-C. (1979). Digital Simulation of Nonlinear Random Waves. *Journal of the Waterway, Port, Coastal and Ocean Division, Proceedings of the American Society of Civil Engineers*, **105**(1 Feb), pp 67-85.
- Kühn, M. (2001). *Dynamics and Design Optimisation of Offshore Wind Energy Conversion Systems*. Dept. of Wind Energy Research Institute, Delft University, Delft
- Machado, U. B. (2002). *Statistical Analysis of Non-Gaussian Environmental Loads and Responses*. Dept. of Centre for Mathematical Sciences Mathematical Statistics Lund Institute of Technology, Lund University, Lund
- Massel, S. R. (1996). *Ocean Surface Waves: Their Physics and Prediction*. Singapore: World Scientific Publishing
- Mei, C. C. (1983). *The applied dynamics of ocean surface waves*. New York: Wiley. 0-471-06407-6
- Nestegård, A. and Stokka, T. (1995). Third-order random wave model. In: *Proceedings of the 5th 1995 International Offshore and Polar Engineering Conference*, (p 136). Hague, Neth, 11-16 Jun.
- Oscar, D. S. and Paez, T. L. (1988). Analysis of Wind Turbines on Offshore Support Structures Excited by Random Wind and Random Waves. In: *Proceedings of the*

- Seventh ASME Wind Energy Symposium. Presented at the Eleventh Annual Energy-Sources Technology Conference and Exhibition.*, (pp. 165-172). New Orleans, LA, USA.
- Rogers, N. (1998). Structural dynamics of offshore wind turbines subject to extreme wave loading. In: Powles, S., *Proceedings of the BWEA 20 Annual Conference 1998 Switch on to Wind Power, 2-4 Sept. 1998*, (pp. 285-92). Cardiff, UK. 1 86058 137 4.
- Ronsten, G., Thor, S., Ganander, H., Johansson, H., Thiringer, T., Petru, T. and Bergström, H. (2000). Evaluation of loads, power quality, grid interaction, meteorological conditions and power performance of the first Swedish offshore wind farm at Bockstigen. In: *Proceedings of the Offshore Wind Energy in Mediterranean and Other European Seas*, (pp. 253-267). Sardinia.
- Sinclair, F. M. (1994). Aerodynamic damping on offshore installations - a comparison of experimental measurements with theory. *Journal of Wind Engineering and Industrial Aerodynamics Proceedings of the Wind Engineering Society Inaugural Conference, Sep 28-30 1992*, **52**(May 1-3), pp 321-344.
- Sjöfartsverket, (1979). Waters Surrounding Gotland. Sea Chart. Edition 79-04, Sjöfartsverket, Norrköping.
- Stansberg, C. T. (1998). Non-Gaussian extremes in numerically generated second-order random waves on deep water. In: *Proceedings of the 8th International Offshore and Polar Engineering Conference*, (pp. 103-110). Montreal, Can, May 24-29.
- Stansberg, C. T. and Gudmestad, O. T. (1996). Non-linear random wave kinematics models verified against measurements in steep waves. In: *Proceedings of the 15th International Conference on OMAE*, (pp. 15-24).
- Tucker, M. J., Carter, D. J. T. and Challenor, P. G. (1984). Numerical Simulation of a Random Sea: A Common Error and Its Effect Upon Wave Group Statistics. *Applied Ocean Research*, **6**(2 Apr), pp 118-122.
- Wahl, G. (1983). *Vågdata och vågeffekt vid svenska kustfarvatten*. Marintekniska institutet SSPA (Rapport 2265-3), Göteborg
- van der Tempel, J. and Molenaar, D.-P. (2002). Wind turbine structural dynamics - A review of the principles for modern power generation, onshore and offshore. *Wind Engineering*, **26**(4), pp 211-220.
- Young, I. R. (1999). *Wind Generated Ocean Waves* (Vol. 2). Oxford: Elsevier Science

Paper A:

Jenny Trumars, Johan Jonsson and Lars Bergdahl,

Extreme Non-Linear Wave Forces on a Monopile in Shallow water,

In: Proceedings of OMAE03, 22ND International Conference on Offshore Mechanics and Arctic Engineering, June 8–13, 2003, Cancun, Mexico

OMAE2003-37049

EXTREME NON-LINEAR WAVE FORCES ON A MONOPILE IN SHALLOW WATER

Jenny M. V. Trumars

Chalmers University of Technology
Water Environment Transport
S 412 96 Göteborg, Sweden
Tel: +46 31 772 2149
Fax: +46 31 772 2128
Email: jenny.trumars@wet.chalmers.se

Johan O. Jonsson

Volvo Technology Corporation/
Chalmers University of Technology
S 412 88 Göteborg, Sweden
Tel: +46 31 322 1223
Fax: +46 31 82 08 87
Email: johan.jonsson@volvo.com

Lars Bergdahl

Chalmers University of Technology
Water Environment Transport
S 412 96 Göteborg, Sweden
Tel: +46 31 772 2155
Fax: +46 31 772 2128
Email:
lars.bergdahl@wet.chalmers.se

ABSTRACT

A phase averaging wave model (SWAN) is used to transform offshore sea states to the near to shore site of an offshore wind energy converter. The supporting structure of the wind turbine consists of a cylindrical monopile, and the wave forces and resulting base moments on it are calculated by Morison's equation integrating from the bottom to the instantaneous free surface. For that purpose the wave-motion in the time domain at the monopile is realized by a second-order random wave model.

Keywords: Non-linear Waves, Wave Load, Wind Energy Converter

INTRODUCTION

As energy production from wind power becomes more common the lack of sites for wind power farms on land is turning into a problem. This has led to an expansion offshore at sites with depths ranging from approximately 6 to 30 m. However, change of location from land to sea changes the design requirements of wind energy converters. In addition to standard loads, the wave load on the structure has to be taken into account. To calculate the wave load at the depths in question, theory for waves at finite depth has to be used.

When waves travel from deep sea towards land they transform due to the influence from bottom topography and bottom friction. Amplitudes and wavelengths decrease and the waves change direction. This transformation can be simulated using phase-averaging models, modelling the local statistical properties of the sea as *e.g.* the variation of directional variance spectra, or using phase resolving models, where the

deterministic properties of the sea *e.g.* the time- and space-varying sea surface elevation is computed. The latter method captures the phenomena of troughs becoming shallower and peaks sharper, which are typical non-linear features of high waves at finite depth. On the other hand, by using statistical properties from a phase-averaging model, a local realization in the time domain can be obtained. However, it is vital that such a realization retains the statistical properties of the sea while reproducing the non-linear features. If non-linearities are of interest, a higher order realization, *e.g.* using a higher order perturbation theory, has to be used.

The sea surface elevation and the velocity potential can be calculated by Fourier sums. The velocity is then calculated as the spatial derivative of the velocity potential. The numerical derivative of the velocity with respect to time gives the acceleration, which together with Morison's equation gives the resulting structural loading.

The problem with waves on offshore wind power plants has been addressed by a number of scientists, including Kühn [1] and Cheng [2]. Kühn used higher-order stream function theory to assess extreme regular waves. Cheng used a random linear wave model to study extreme responses. In this paper we use a second-order realization of non-linear waves based on a wave spectrum at a wind farm site. Results from the second-order realization are compared with results from a first-order realization. The on-site spectrum is calculated with help of the phase averaging model SWAN (Simulating WAVes Nearshore).

The example site is the offshore wind power farm at Bockstigen, which is situated off the coast of the Swedish island of Gotland in the Baltic Sea. See Fig. 1 and 2. One of the wind energy converters at the wind power farm is subject to an extensive measurement program including measurements of waves, wind and the structural response of the structure.

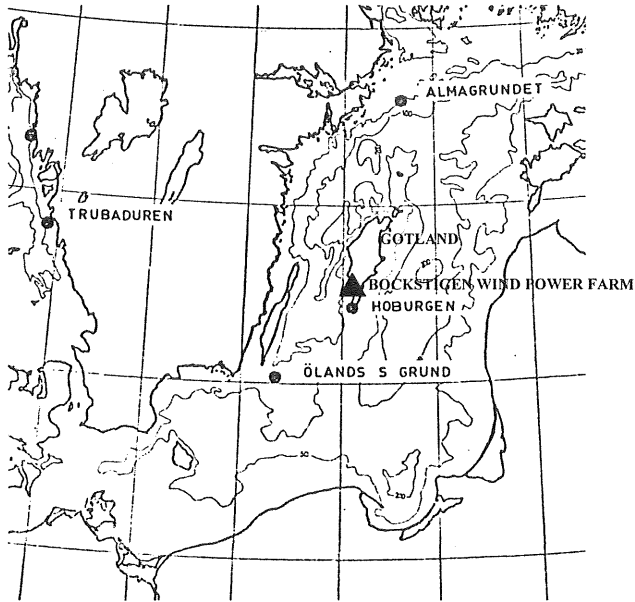


Figure 1. The Baltic Proper with the location of Bockstigen marked with a triangle.

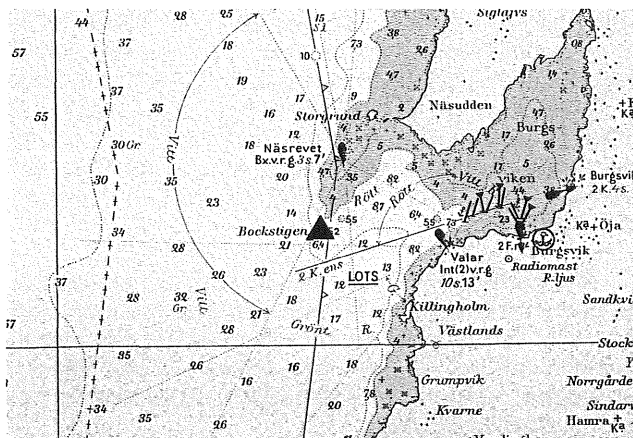


Figure 2. A detailed close-up at the location of Bockstigen off the coast of Gotland.

The support structure of the wind turbine is a tower mounted on a cylindrical steel monopile drilled into the limestone and extending above the water surface. The cylinder diameter is 2.1 m and the mean-water depth is 6.5 m at the site. See Fig. 3.

The wave climate in the Baltic Sea was studied during 1978 to 1982 by SSPA [3]. Here, mean spectra have been

derived from these measurements. In this study a spectrum for a wind speed of 20 m/s and open sea, at Ölands Södra Grund, see Fig. 1, was chosen as input to the SWAN model. The dominant wind direction is from the South West and this is in line with the longest fetch.

The choice of computational model was based on accessibility in form of open source code and economy. As speed of computation was important SWAN was chosen. To capture the second-order characteristics a second-order realization of the waves was applied.

METHOD

SWAN

SWAN (Simulating Waves Nearshore) [4] is a phase averaging wave model where the statistical properties of the waves are calculated. It accounts for wave propagation processes, *e.g.* refraction, shoaling and transmission through sub-grid obstacles; wave generation by wind; and wave dissipation by whitecapping, depth-induced wave breaking and bottom friction. It also handles wave-wave interactions. SWAN uses a finite difference scheme.

SWAN requires bottom topography, wind and wind direction as input. Spectra with directional spreading are used at the model boundaries. Results at the site of the wind power plant are significant wave height, frequency spectrum and directional spectrum.

Extreme waves at the wind power farm were obtained by using an extreme sea state as input to SWAN. Due to extensive calculation time of the Fourier sums in the second-order realization, the obtained spectrum at the site was initially used as a basis for several first-order realizations in time over a one-minute period. Thereafter a realization containing a statistical maximum wave, H_{max} was chosen. [5]

$$H_{max} = 7.7 \sqrt{m_0} \quad (1)$$

Here m_0 denotes the zeroth moment of the spectrum or the variance of the water elevation

$$m_0 = \int_0^{\infty} S(\omega) d\omega. \quad (2)$$

The phases in the chosen first-order realization was then used in a second-order realization. If H_{max} of the second-order realization was greater than $0.78 h$, which is the depth-breaking limit for the waves [6], the realization was discarded and another realization was chosen.

Second-order realization of waves

The boundary value problem for the irrotational flow of surface gravity waves in an incompressible, homogeneous and inviscid fluid can be expressed in terms of a velocity potential $\Phi(x,z,t)$. The water particle velocities are given by the spatial derivative of Φ as

$$u = -\Phi_x \quad (3)$$

$$w = -\Phi_z \quad (4)$$

where the subscript denotes partial differentiation.

The coordinate system is chosen so that the positive, vertical z-axis is pointing upwards and the x-axis is in line with the still water surface at $z=0$. For notation see Fig. 3. The governing differential equation is the Laplace equation

$$\nabla^2 \Phi = 0 \quad \text{for} \quad -h \leq z \leq \eta(x,t). \quad (5)$$

With the boundary conditions given by

$$\Phi_z = 0 \quad \text{for} \quad z = -h, \quad (6)$$

$$g\eta - \Phi_t + \frac{|\bar{\nabla}\Phi|^2}{2} = 0 \quad \text{for} \quad z = \eta(x,t) \quad (7)$$

where g is the acceleration of gravity and

$$\eta_t - \bar{\nabla}\Phi \cdot \bar{\nabla}\eta + \Phi_z = 0 \quad \text{for} \quad z = \eta(x,t). \quad (8)$$

The velocity potential and the free surface elevation η can, for small waves, be expressed as perturbation expansions

$$\Phi(x,z,t) = \sum_{j=1} \Phi_j(x,z,t) \quad \text{for} \quad -h \leq z \leq 0, \quad t > 0 \quad (9)$$

and

$$\eta(x,t) = \sum_{j=1} \eta_j(x,t) \quad \text{for} \quad t > 0 \quad (10)$$

where j denotes the perturbation ordering parameter.

The first-order perturbation equations can be written as

$$\nabla^2 \Phi_1 = 0 \quad \text{for} \quad -h \leq z \leq 0, \quad (11)$$

$$\Phi_{1z} = 0 \quad \text{for} \quad z = -h, \quad (12)$$

$$\eta_1 = \frac{1}{g} \Phi_{1t} \quad \text{for} \quad z = 0 \quad (13)$$

and

$$\eta_{1t} = -\Phi_{1z} \quad \text{for} \quad z = 0. \quad (14)$$

The solution to the linear problem can be expressed by the Fourier series

$$\Phi_1(x,z,t) = -i \sum_{m=0}^N F(m) \frac{g}{\omega_m} \frac{\cosh[k_m(z+h)]}{\cosh(k_m h)} \exp i(\omega_m t - k_m x) \quad (15)$$

and

$$\eta_1(x,t) = \sum_{m=0}^N F(m) \exp i(\omega_m t - k_m x), \quad (16)$$

where the wave number k is given by the dispersion relation

$$\omega_m^2 = gk_m \tanh k_m h, \quad (17)$$

i is the imaginary unit, ω is the angular frequency, g is the acceleration of gravity and h is the water depth.

The second-order perturbation equations may be written as

$$\nabla^2 \Phi_2 = 0 \quad \text{for} \quad -h \leq z \leq 0, \quad (18)$$

$$\Phi_{2z} = 0 \quad \text{for} \quad z = -h, \quad (19)$$

$$\eta_{2t} + \Phi_{2z} = \Phi_{1x} \eta_{1x} - \Phi_{1z} \eta_{1z} \quad \text{for} \quad z = 0 \quad (20)$$

and

$$g_2 \eta_{2t} - \Phi_{2t} = -\frac{1}{2} \left(\Phi_{1x}^2 + \Phi_{1z}^2 \right) + \Phi_{1z} \eta_{1z} \quad (21)$$

for $z = 0$.

The solution to the second-order problem becomes

$$\Phi_2(x,z,t) = -i \sum_{n=0}^N \sum_{m=0}^N F(n) F(m) D(\omega_n, \omega_m) \frac{\cosh[(k_n + k_m)(z+h)]}{\cosh[(k_n + k_m)h]} \exp i[(\omega_n + \omega_m)t - (k_n + k_m)x] \quad (22)$$

and

$$\eta_2(x,t) = \sum_{n=0}^N \sum_{m=0}^N \frac{F(n) F(m)}{2g} H(\omega_n, \omega_m) \exp i[(\omega_n + \omega_m)t - (k_n + k_m)x] \quad (23)$$

where

$$D(\omega_n, \omega_m) = \frac{\Omega(\omega_n, \omega_m)}{X(\omega_n, \omega_m)}, \quad (24)$$

$$\Omega(\omega_n, \omega_m) = 2(\omega_n + \omega_m) \left[g^2 k_n k_m - (\omega_n \omega_m)^2 \right] - \omega_n \omega_m (\omega_n^3 + \omega_m^3) + g^2 (\omega_m k_n^2 + \omega_n k_m^2) \quad (25)$$

$$X(\omega_n, \omega_m) = 2\omega_n \omega_m \left[(\omega_n + \omega_m)^2 - g(k_n + k_m) \tanh(k_n + k_m)h \right] \quad (26)$$

and

$$H(\omega_n, \omega_m) = 2(\omega_n + \omega_m) D(\omega_n, \omega_m) - \frac{g^2 k_n k_m}{\omega_n \omega_m} + (\omega_n + \omega_m)^2 - \omega_n \omega_m \quad (27)$$

The complex amplitude $F(n)$ is given by

$$F(n) = \sqrt{2S(\omega_n)\Delta\omega} \exp(-i\varepsilon_n) \quad (28)$$

where S is the variance density spectrum, $\Delta\omega$ is the frequency resolution and ε a random phase angle distributed between 0 and 2π . The use of the variance density spectrum for calculating the complex amplitudes retains the statistical properties of the sea.

Equations 3 through 28 are valid for finite depth and small waves [7], [8] and [9].

Calculation of water velocities

In order to prevent the calculated velocities above the still water level from becoming unrealistically high, an approximation to the wave particle kinematics is implemented by a Taylor expansion to the first order around $z = 0$ [10]. This approximation is used for both the first and second-order realization.

$$u(x, z, t) = \Phi_x \Big|_{z=0} + \Phi_{xz} \Big|_{z=0} z \quad (29)$$

The water particle velocities are then given by Eq. 3 and 4.

Computation of structural forces and moments

The wave forces P and resulting base moment M on the monopile are calculated by using Morison's equation integrating from the bottom to the instantaneous free surface

$$P = \frac{1}{2} \rho C_D D \int_{-h}^{\eta} u |u| dz + \rho \frac{\pi D^2}{4} C_M \int_{-h}^{\eta} u_t dz \quad (30)$$

and

$$M = \frac{1}{2} \rho C_D D \int_{-h}^{\eta} u |u| (z+h) dz + \rho \frac{\pi D^2}{4} C_M \int_{-h}^{\eta} u_t (z+h) dz \quad (31)$$

Where C_D is the drag coefficient, C_M is the inertia coefficient, ρ is the water density and D is the diameter of the monopile [11]. Figure 3 depicts the monopile.

The monopile is considered to be a rigid structure and also hydrodynamically transparent, that is the waveform is not affected by the presence of the structure. This is valid when the structure diameter to wavelength ratio is small. [12]

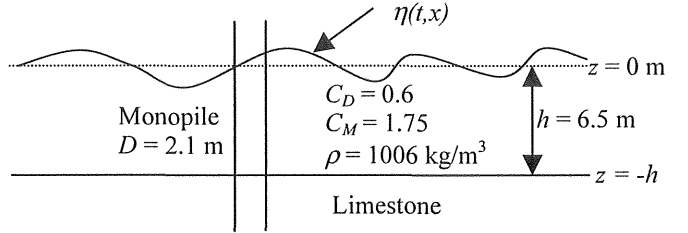


Figure 3. Details of the monopile. The monopile extends above the sea surface and the water depth is 6.5 meters. η is the instantaneous free water surface and the dotted line is the still water level.

RESULT

The realization was made over a time of 63 seconds and the sea surface elevation, force and base moment from both the first and second-order realisation have been calculated throughout that time period. Around $t = 22$ s velocities, accelerations and forces along the monopile have been calculated.

Figure 4 shows the total sea surface elevation and the first and second-order contributions to it. At the end of the realised time history, $t = 60$ s, the wave takes the ideal form and the trough before the peak has become more shallow compared to the first-order simulation and the peak is sharper. The result at $t = 20$ s shows an overshoot of the second-order contribution resulting in a trough below the first-order realisation. This could indicate that the simulated waves are violating the small amplitude requirement.

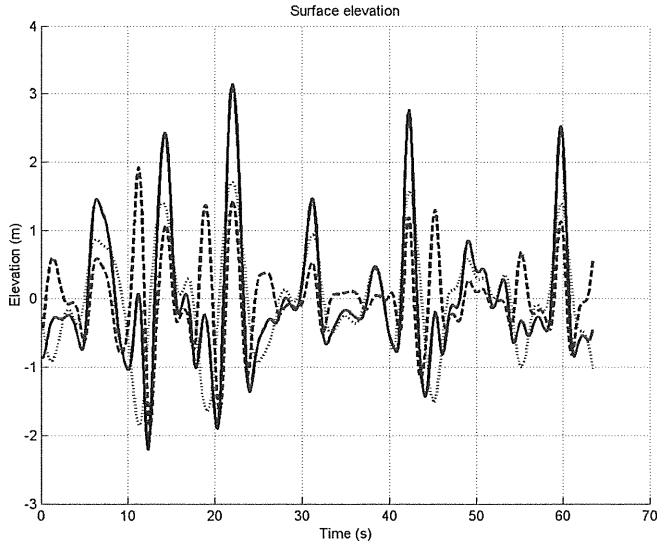


Figure 4. Surface elevation in meters. The solid line represents the total elevation, the dotted line shows the first-order contribution and the dashed line shows the second-order contribution.

The forces and base moments are calculated according to Eq. (30) and (31) throughout the time series. Figure 5 and 6 shows the surface elevation compared to the force and base moments for the first and second-order realisation respectively. The force is scaled down by 10^5 and the moment with 10^6 in order to get a clear picture of when they have a maximum or minimum compared with the sea surface elevation. The maximum force and base moment is at the zero up crossing of the highest wave.

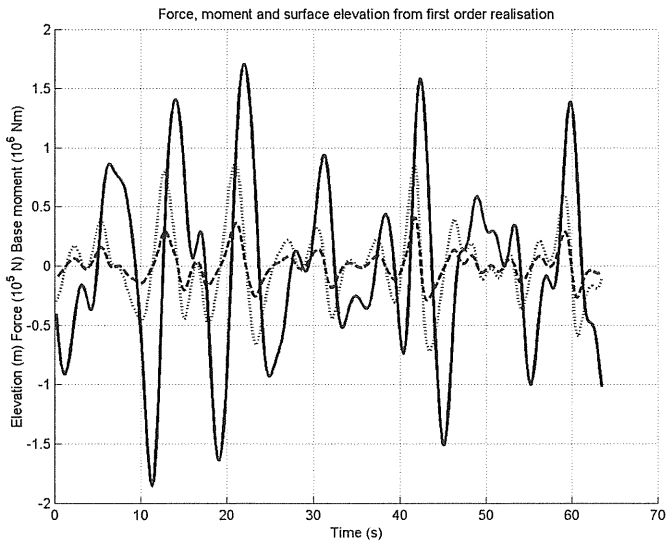


Figure 5. The surface elevation compared to the force and the base moments calculations from the first-order realization. The solid line shows the total elevation (m), the dotted line shows the force (10^5 N) and the dashed line shows the base moment (10^6 Nm).

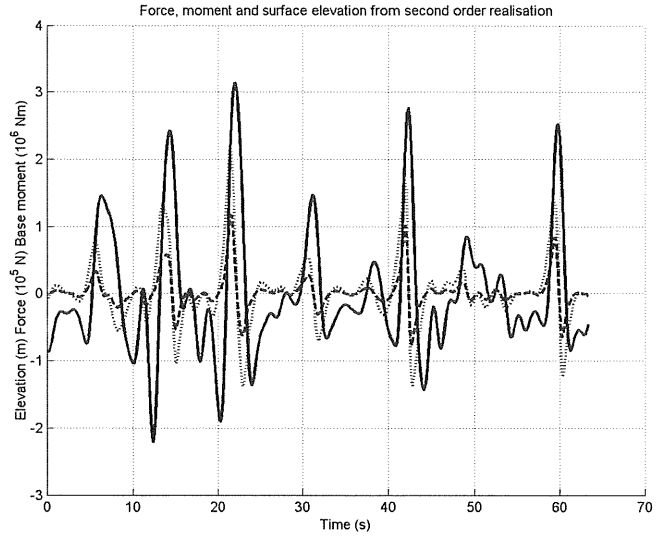


Figure 6. The surface elevation compared to the force and the base moments calculations from the second-order realization. The solid line shows the total elevation (m), the dotted line shows the force (10^5 N) and the dashed line shows the base moment (10^6 Nm).

From a comparison of the results from the first and second-order realisation in Fig. 7 and 8 it can be seen that the second-order realisation yields higher loads. Higher particle velocities and the fact that a larger portion of the structure is submerged in the second order-realisation cause this.

For the comparison of the elevations the ratio A_{max}/H_{max} was studied. A_{max} is the positive amplitude for the maximum wave and H_{max} is the corresponding wave height. When the troughs are becoming shallower and the peaks sharper for the second order realisation, showing asymmetry around the still water level, this ratio increases. This effect can also be studied in the force and the base moment, see Table 1. However, it is not as pronounced as for the elevation. When calculating the ratio for the force and base moment H_{max} is the maximum trough to peak value and A_{max} is the corresponding positive amplitude.

Table 1. The ratio A_{max}/H_{max}

Order of realisation	First	Second
Elevation	0.51	0.62
Force	0.57	0.61
Base moment	0.58	0.65

The force and base moment display asymmetry around zero for the first-order realisation and it is increased further for the second-order realisation. In the first-order case the asymmetry is caused by the use of Morison's equation integrating from the bottom to the instantaneous free surface, Eq. 30 and 31, and the higher particle velocities at the crests of the waves.

For a large number of realisations over longer times the mean of the ratio for the first-order wave elevation will be 0.5.

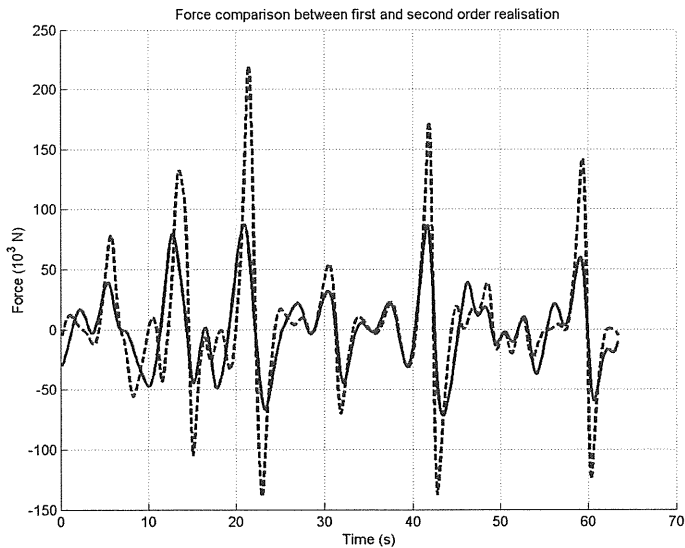


Figure 7. Comparison of the force (10^3 N) from the first and second-order realization. The solid line shows the result from the first-order realization and the dashed line shows the result from the second-order realization.

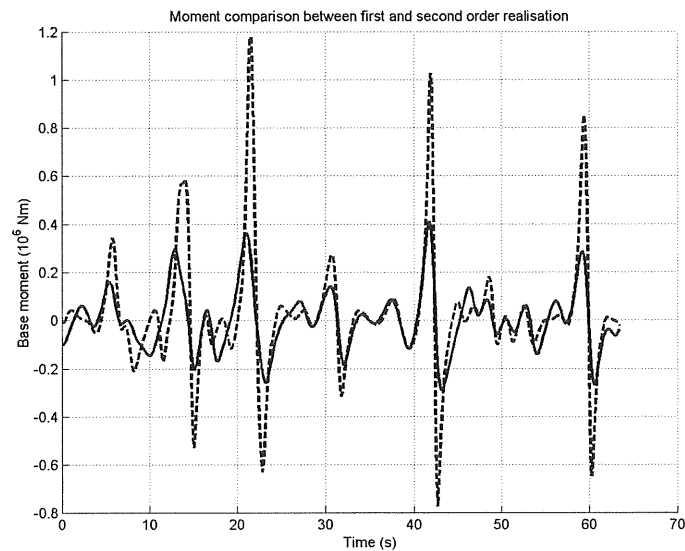


Figure 8. Comparison of the base moment (10^6 Nm) from the first and second-order realization. The solid line shows the result from the first-order realization and the dashed line shows the result from the second-order realization.

When calculating forces distributed along the monopile focus is on the highest peak, at $t = 22$ s, of the surface elevation in Fig. 4. Velocities and accelerations were calculated at half meter intervals starting from the sea bottom, $z = -6.5$ m. The results are shown in Fig. 9 and 10. The loading force was calculated in the middle of each interval, see Fig. 11. The times of the calculations were chosen around the highest peak. They coincide with the trough $t = 20.3$ s, zero up crossing $t = 21$ s, peak $t = 22$ s and zero down crossing $t = 23$ s of the surface elevation. Studying the distribution along the monopile, one

finds that the highest velocity is at the peak and the highest acceleration and force is at the zero down crossing.

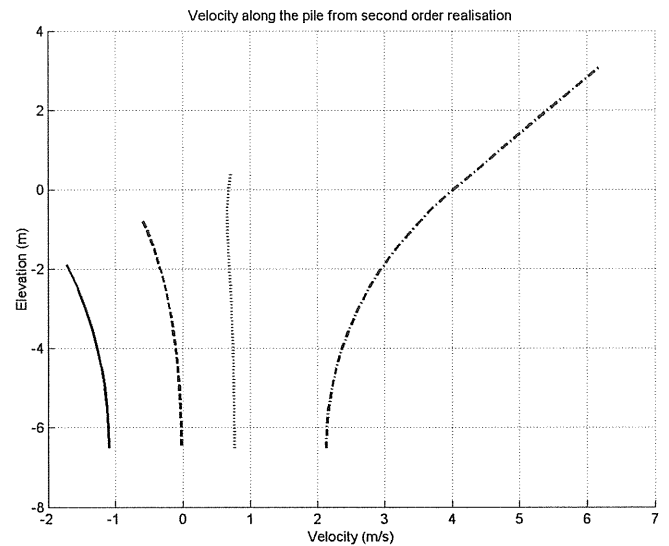


Figure 9. Velocity as a function of surface elevation. The solid line shows velocity at $t = 20.3$ s, the dashed line at $t = 21$ s, the dot dashed line at $t = 22$ s and the dotted line at $t = 23$ s.

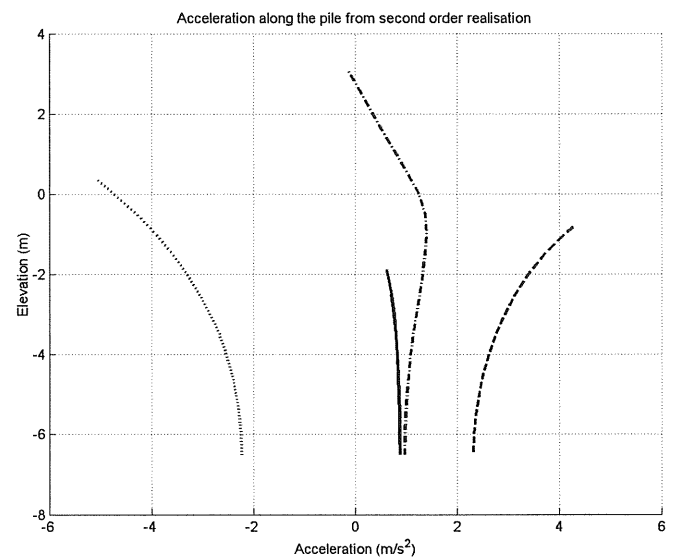


Figure 10. Acceleration as a function of surface elevation. The solid line shows acceleration at $t = 20.3$ s, the dashed line at $t = 21$ s, the dot dashed line at $t = 22$ s and the dotted line at $t = 23$ s.

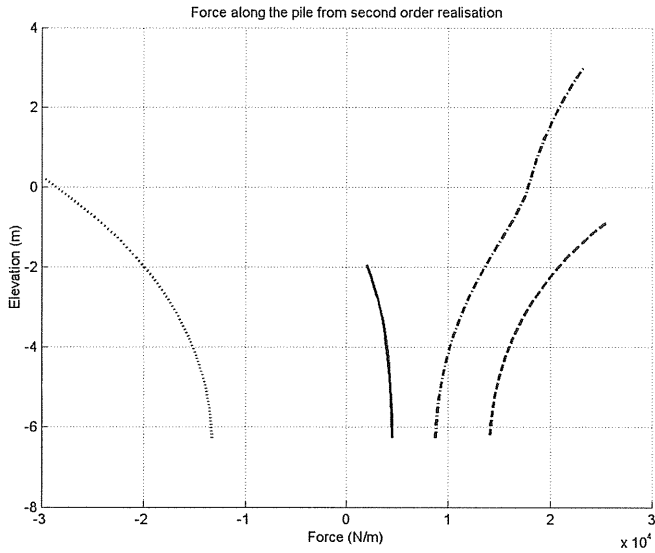


Figure 11. Distributed force as a function of surface elevation. The solid line shows force at $t = 20.3$ s, the dashed line at $t = 21$ s, the dot dashed line at $t = 22$ s and the dotted line at $t = 23$ s.

CONCLUDING REMARKS

This method provides a way of calculating non-linear irregular waves at finite depths. In earlier investigations only regular higher-order Stokes waves or solitary waves have been taken into account.

In the calculation care has to be taken not to violate the limitations of the methods. It is important to test the small wave requirement of the perturbation series. Stansberg e.g. [13] enforces a restriction based on keeping third-order omitted terms smaller than the corresponding second-order terms to avoid unrealistically large local wave steepness with associated velocities and accelerations, which otherwise would result in non-physical forces. This results in a restriction on the wave number and consequently on the angular frequency. The restriction can be implemented by a cut-off at the high frequency end of the input spectrum. A discussion on the largest wave height in water of constant depth can be found in [14]. The limiting value for H_{max} of $0.55 h$ is found to apply to shallow water waves. This is a more restrictive value than the breaker height limit $0.78 h$ for mildly shoaling bottoms used in the calculation above. The implication is that for shoaling cases $0.78 h$ should be used and for vast shallows $0.55 h$ may be more accurate but less conservative.

It is observed that the calculated forces and base moments are highest at the crest of the waves. High particle velocities and the fact that a larger portion of the structure is submerged at the crest explain this. It is also observed that the second-order realization gives larger maximum forces and base moments than the first-order realization due to the higher wave crests.

Implementing a Fast Fourier Transform (FFT) method can make the Fourier sums faster which would allow a larger

number of simulations over longer time-periods and statistical analysis of the results.

Validation of the wave and load calculations will be carried out within the measurement program at Bockstigen. The loading on the structure has to be derived from the measured internal load effects (structural shear forces and moments), and consequently the flexibility of the structure has then to be considered.

ACKNOWLEDGMENTS

The financial support given by the Swedish Energy Agency is gratefully acknowledged.

REFERENCES

- [1] Kühn M. J., 2001, "Dynamics and Design Optimisation of Offshore Wind Energy Conversion Systems", Ph.D. thesis, DUWIND Delft University Wind Energy Research Institute, Delft, pp. 60-71 97-103
- [2] Cheng P. W., 2002, "A Reliability Based Design Methodology for Extreme Responses of Offshore Wind Turbines", Ph.D. thesis, DUWIND Delft University Wind Energy Research Institute, Delft, pp. 17-35 43-48
- [3] Wahl G., 1983, "Vågdata och vågeffekt vid svenska kustfarvatten", Rapport 2265-3, Marintekniska institutet SSPA, Göteborg
- [4] Holthuijsen L. H., Booij N., Ris R. C., Haagsma IJ. G., Kieftenburg A. T. M. M., Kriezi E. E., 2000, "SWAN Cycle III version 40.11, USER MANUAL" Delft University, Delft
- [5] Beck R. P., Cummins W. E., Dalzell J.F., Mandel P., Webster W. C., 1989, "Principles of Naval Architecture, Volume 3, Motions in Waves and Controllability", The Society of Naval Architects and Marine Engineers, Jersey City, pp 17-21
- [6] 1977, "Shore Protection Manual, Volume 1", U.S Army Coastal Engineering Research Center, Fort Belvoir, pp 2-121
- [7] Hasselmann K., 1962, "On the non-linear energy transfer in a gravity-wave spectrum, Part 1 General theory", *Journal of Fluid Mechanics*, 12, pp 481-500
- [8] Hudspeth R. T., Chen M., 1979, "Digital Simulation of Nonlinear Random Waves" *Journal of the Waterway Port Coastal and Ocean Division*, 105, pp 67-85
- [9] Machado U. E. B., 2002, "Statistical Analysis of Non-Gaussian Environmental Loads and Responses" Ph.D. thesis, Lund University of Technology, Lund
- [10] Nestegård A., Stokka T., 1995, "A third order random wave model", *Proc., 5th International Offshore and Polar Engineering Conference, The Hague, The Netherlands, June 11-16*, pp 136-142
- [11] Moberg G., 1988, "Wave Forces on a Vertical Slender Cylinder", Ph.D. thesis, Chalmers University of Technology, Göteborg, pp 36
- [12] 1984, "Shore Protection Manual, Volume 2", Department of the Army Waterways Experiment Station, Corps of Engineers, Vicksburg, pp 7-103
- [13] Stansberg C. T., 1998 "Non-Gaussian Extremes in Numerically Generated Second-Order Random Waves on Deep Water", *Proc., Eighth International Offshore and Polar Engineering Conference, Montréal, Canada, May 24-29*, pp 103-110
- [14] Massel S. R., 1996, "Ocean Surface Waves: Their Physics and Prediction", World Scientific Publishing, Singapore, pp 284-305

Paper B:

Jenny Trumars, Johan Jonsson and Lars Bergdahl,

The Effect of Wave Non-Linearity on the Forces on a Wind Turbine Foundation in Shallow Water,

In: Proceedings of EWEC 2003, European Wind Energy Conference & Exhibition, June 16 – 19, 2003, Madrid, Spain

The Effect of Wave Non-Linearity on the Forces on a Wind Turbine Foundation in Shallow Water

Jenny M. V. Trumars¹, Johan O. Jonsson², Lars Bergdahl³

¹ Chalmers University of Technology, Water Environment Transport, S 412 96 Göteborg, Sweden, Tel: +46 31 772 2149, Fax: +46 31 772 2128, Email: jenny.trumars@wet.chalmers.se

² Volvo Technology Corporation/ Chalmers University of Technology

³ Chalmers University of Technology, Water Environment Transport

Abstract

A phase-averaging wave model (SWAN) is used to transform sea states in intermediate waters to the near-to-shore site of a wind-power plant. The supporting structure of the wind-power plant consists of a cylindrical monopile. The wave forces and resulting base moments on it are calculated by Morison's equation integrating from the bottom to the instantaneous free surface. For that purpose the wave-motion at the monopile is realised by a non-linear random wave model. Comparisons are made with a linear random wave model. The effect of the non-linear realisation on the variance of the surface elevation and the loads is studied. The relevance of using a non-linear realisation is discussed with respect to the effect on the calculated loads. The purpose of the study is to see how important it is to use a non-linear approach when assessing wave loads in shallow water.

Keywords: Non-linear Waves, Wave Load, Wind Energy Converter

Introduction

The lack of sites for wind power farms on land is turning into a problem as energy-production from wind power becomes more common. This has led to a development offshore at sites with depths ranging from approximately 6 to 30 m. Because of the shift of location from land to sea there is a change in the design requirements of wind energy converters as, in addition to standard loads, also the wave load on the structure has to be taken into account. For the sites in question theories for waves at finite depth must be used in order to calculate the wave load.

Due to the influence from bottom topography and bottom friction waves transform as they travel from deep sea towards land. The waves change direction and the amplitudes and wavelengths decrease. The transformation of the waves can be calculated with phase-averaging models, in which the local statistical properties of the sea as *e.g.* the variation of directional variance spectra, or with phase resolving models, in which the deterministic properties of the sea *e.g.* the time- and space-varying sea surface elevation is computed. The phase resolving models capture the phenomena of troughs becoming shallower and peaks sharper, which are typical non-linear features of high waves at finite depth. On the other hand, by using statistical properties from a phase-averaging model, a local realisation in the time domain can be obtained by a Fourier sum. It is vital that such a realisation retains the statistical properties of the sea while reproducing the non-linear features, and therefore some higher order realisation, *e.g.* using a higher order perturbation theory, has to be used.

The sea surface elevation and the velocity potential can be calculated by Fourier sums. Subsequently the water particle velocity in any point in the water can be calculated as the spatial derivative of the velocity potential and then the numerical derivative of the velocity with respect to time gives the associated acceleration. Finally the calculated velocity and acceleration are inserted in Morison's equation to yield the resulting structural loading.

The problem with waves on offshore wind power plants has been addressed by a number of scientists, including Kühn [1] and Cheng [2]. Kühn used higher-order stream function theory to assess extreme regular waves. Cheng used a random linear wave model to study extreme responses. Hendersson and Cheng have studied non-linear-random waves and wave loads at Blyth [3]. In this paper we use a second-order realisation of non-linear waves based on a wave spectrum at a wind farm site. Results from the non-linear realisation are compared with results from a linear realisation. The on-site spectrum is calculated with help of the phase averaging model SWAN (Simulating WAVes Nearshore). [4]

The example site is the offshore wind power farm at Bockstigen, which is situated off the coast of the Swedish island of Gotland in the Baltic Sea. See fig. 1 and 2. One of the wind energy converters at the wind power farm is subject to an extensive measurement program including measurements of waves, wind and the structural response of the structure.



Figure 1. The Baltic Proper with the location of Bockstigen marked with an arrow.



Figure 2. A detailed close-up at the location of Bockstigen off the coast of Gotland.

The support structure of the wind turbine is a tower mounted on a cylindrical steel monopile drilled into the limestone and extending above the water surface. The cylinder diameter is 2.1 m and the mean-water depth is 6.5 m at the site. See fig. 3.

The wave climate in the Baltic Sea was studied during 1978 to 1982 by SSPA [5]. Here, mean spectra have been derived from these measurements. In this study a spectrum for a wind speed of 20 m/s and open sea, at Ölands Södra Grund, see fig. 1, was chosen as input to the SWAN model. The dominant wind direction is from the South West and this is in line with the longest fetch.

The phase averaging computational model SWAN was chosen based on accessibility in form of open source code, economy, and speed of computation. To capture the non-linear characteristics of the waves time realisations to the second-order were applied.

Method

SWAN

SWAN (Simulating WAVes Nearshore) is a phase averaging wave model where the statistical properties of the waves are calculated. It accounts for wave propagation processes, e.g. refraction, shoaling and transmission through sub-grid obstacles; wave generation by wind; and wave dissipation by whitecapping, depth-induced wave breaking and bottom friction. It also handles wave-wave interactions. SWAN uses a finite difference scheme.

SWAN requires bottom topography, wind and wind direction as input. Spectra with directional spreading are used at the model boundaries. Results at the site of the wind power plant are significant wave height, frequency spectrum and directional spectrum.

Extreme waves at the wind power farm were obtained by using an extreme deep-water sea state as input at the seaward boundary in SWAN.

Non-linear realisation of waves

The non-linear realisation of waves is made by calculating the time-series of the waves using first and second-order perturbation expansions of the free surface boundary conditions. These expansions can be expressed as Fourier sums and are added to yield the total non-linear time-series. The first-order perturbation expansion gives the linear realisation. A Fast Fourier Transform (FFT) method has been implemented to calculate the Fourier sums allowing large number of simulations over long time-periods and statistical analysis of the results.

The boundary value problem for the irrotational flow of surface gravity waves in an incompressible, homogeneous and inviscid fluid can be expressed in terms of a velocity potential $\Phi(x,z,t)$. The water particle velocities are given by the spatial derivative of Φ as

$$u = -\Phi_x \quad \text{Equation 1}$$

$$w = -\Phi_z \quad \text{Equation 2}$$

where the subscript denotes partial differentiation.

The coordinate system is chosen so that the positive, vertical z-axis is pointing upwards and the x-axis is in line with the still water surface at $z = 0$. For notation see fig. 3. The governing differential equation is the Laplace equation

$$\nabla^2 \Phi = 0 \quad \text{for} \quad -h \leq z \leq \eta(x,t). \quad \text{Equation 3}$$

With the boundary conditions given by

$$\Phi_z = 0 \quad \text{for} \quad z = -h, \quad \text{Equation 4}$$

$$g\eta - \Phi_t + \frac{|\vec{\nabla}\Phi|^2}{2} = 0 \quad \text{for} \quad z = \eta(x,t) \quad \text{Equation 5}$$

where g is the acceleration of gravity and

$$\eta_t - \vec{\nabla}\Phi \cdot \vec{\nabla}\eta + \Phi_z = 0 \quad \text{for} \quad z = \eta(x,t). \quad \text{Equation 6}$$

The velocity potential and the free surface elevation η can, for small waves, be expressed as perturbation expansions

$$\Phi(x,z,t) = \sum_{j=1}^{\infty} \Phi_j(x,z,t) \quad \text{for} \quad -h \leq z \leq 0, \quad t > 0 \quad \text{Equation 7}$$

and

$$\eta(x, t) = \sum_{j=1} \eta_j(x, t) \quad \text{for} \quad t > 0 \quad \text{Equation 8}$$

where j denotes the perturbation ordering parameter.
The first-order perturbation equations can be written as

$$\nabla^2 \Phi_1 = 0 \quad \text{for} \quad -h \leq z \leq 0, \quad \text{Equation 9}$$

$$\Phi_{1z} = 0 \quad \text{for} \quad z = -h, \quad \text{Equation 10}$$

$$\eta_1 = \frac{1}{g} \Phi_{1t} \quad \text{for} \quad z = 0 \quad \text{Equation 11}$$

and

$$\eta_{1t} = -\Phi_{1z} \quad \text{for} \quad z = 0. \quad \text{Equation 12}$$

The solution to the linear problem can be expressed by the Fourier series

$$\Phi_1(x, z, t) = -i \sum_{m=0}^N F(m) \frac{g}{\omega_m} \frac{\cosh[k_m(z+h)]}{\cosh(k_m h)} \exp i(\omega_m t - k_m x) \quad \text{Equation 13}$$

and

$$\eta_1(x, t) = \sum_{m=0}^N F(m) \exp i(\omega_m t - k_m x), \quad \text{Equation 14}$$

where the wave number k is given by the dispersion relation

$$\omega_m^2 = g k_m \tanh k_m h, \quad \text{Equation 15}$$

i is the imaginary unit, ω is the angular frequency and h is the water depth.

The second-order perturbation equations may be written as

$$\nabla^2 \Phi_2 = 0 \quad \text{for} \quad -h \leq z \leq 0, \quad \text{Equation 16}$$

$$\Phi_{2z} = 0 \quad \text{for} \quad z = -h, \quad \text{Equation 17}$$

$$\eta_{2t} + \Phi_{2z} = \Phi_{x1} \eta_{x1} - \Phi_{zz1} \eta \quad \text{for} \quad z = 0 \quad \text{Equation 18}$$

and

$$g_2 \eta_{-2} \Phi_t = -\frac{1}{2} \left({}_1\Phi_x^2 + {}_1\Phi_z^2 \right) {}_1\Phi_{tz} \eta \quad \text{for} \quad z = 0. \quad \text{Equation 19}$$

The solution to the second-order problem becomes

$${}_2\Phi(x, z, t) = -i \sum_{n=0}^N \sum_{m=0}^N F(n) F(m) D(\omega_n, \omega_m) \frac{\cosh[(k_n + k_m)(z + h)]}{\cosh[(k_n + k_m)h]} \exp i[(\omega_n + \omega_m)t - (k_n + k_m)x] \quad \text{Equation 20}$$

and

$${}_2\eta(x, t) = \sum_{n=0}^N \sum_{m=0}^N \frac{F(n) F(m)}{2g} H(\omega_n, \omega_m) \exp i[(\omega_n + \omega_m)t - (k_n + k_m)x], \quad \text{Equation 21}$$

where

$$D(\omega_n, \omega_m) = \frac{\Omega(\omega_n, \omega_m)}{X(\omega_n, \omega_m)}, \quad \text{Equation 22}$$

$$\Omega(\omega_n, \omega_m) = 2(\omega_n + \omega_m) \left[g^2 k_n k_m - (\omega_n \omega_m)^2 \right] - \omega_n \omega_m (\omega_n^3 + \omega_m^3) + g^2 (\omega_m k_n^2 + \omega_n k_m^2), \quad \text{Equation 23}$$

$$X(\omega_n, \omega_m) = 2\omega_n \omega_m \left[(\omega_n + \omega_m)^2 - g(k_n + k_m) \tanh(k_n + k_m)h \right] \quad \text{Equation 24}$$

and

$$H(\omega_n, \omega_m) = 2(\omega_n + \omega_m) D(\omega_n, \omega_m) - \frac{g^2 k_n k_m}{\omega_n \omega_m} + (\omega_n + \omega_m)^2 - \omega_n \omega_m. \quad \text{Equation 25}$$

The complex amplitude $F(n)$ is given by

$$F(n) = \sqrt{2S(\omega_n)\Delta\omega} \exp(-i\varepsilon_n) \quad \text{Equation 26}$$

where S is the variance density spectrum, $\Delta\omega$ is the frequency resolution and ε a random phase angle distributed between 0 and 2π . The use of the variance density spectrum for calculating the complex amplitudes should retain the statistical properties of the sea.

Equations 3 through 26 are valid for finite depth and small waves [6], [7] and [8].

Calculation of water velocities

In order to prevent the calculated velocities above the still water level from becoming unrealistically high, an approximation to the wave particle kinematics is implemented by a Taylor expansion to the first order around $z = 0$ [9]. This approximation is used for both the first and second-order realisation.

$$u(x, z, t) = \Phi_x \Big|_{z=0} + \Phi_{xz} \Big|_{z=0} z . \quad \text{Equation 27}$$

The water particle velocities are then given by eq. 3 and 4.

Computation of structural forces and moments

The wave forces P and resulting base moment M on the monopile are calculated by using Morison's equation integrating from the bottom to the instantaneous free surface

$$P = \frac{1}{2} \rho C_D D \int_{-h}^{\eta} u |u| dz + \rho \frac{\pi D^2}{4} C_M \int_{-h}^{\eta} u_t dz \quad \text{Equation 28}$$

and

$$M = \frac{1}{2} \rho C_D D \int_{-h}^{\eta} u |u| (z+h) dz + \rho \frac{\pi D^2}{4} C_M \int_{-h}^{\eta} u_t (z+h) dz . \quad \text{Equation 29}$$

Where C_D is the drag coefficient, C_M is the inertia coefficient, ρ is the water density and D is the diameter of the monopile [10]. Figure 3 depicts the monopile.

The monopile is considered to be a rigid structure and also hydrodynamically transparent, that is the waveform is not affected by the presence of the structure. This is valid when the structure diameter to wavelength ratio is small. [11]

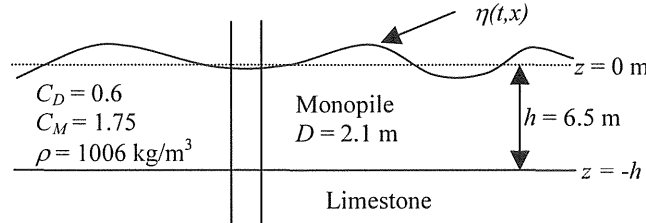


Figure 3. Details of the monopile. The monopile extends above the sea surface and the water depth is 6.5 meters. η is the instantaneous free water surface and the dotted line is the still water level.

Sample simulations

The realisations were made based on the spectrum obtained from SWAN. Ten linear and non-linear realisations of one hour duration were made and the forces on the structure were calculated for all ten cases. Variance and power-spectra for elevation, force and base bending-moment were calculated from the obtained time-series. The mean and standard deviation for the spectra were calculated and the spectra were smoothed. For the linear time-series the standard deviation of the spectra is small. Computing the non-linear realisation of the waves there is an increase in the variance of the sea-surface elevation compared to the first-order linear case. Stansberg [12] also get an increase when calculating non-linear deep-water waves but to a much lesser degree. The increase is due to the addition of higher frequency components in the non-linear realisations, as can be seen in fig. 8. The increase in variance produces unrealistically high waves, exceeding the wave-breaking limit of $0.78 h$ [13], which in this case is 5.07 meters. It can also be observed that the spectrum is broadbanded and produces ripples. See fig 4. For waves below the wave-breaking limit the waves and the forces exhibit the desired non-linear effects of troughs becoming shallower and the peaks sharper, fig 5.

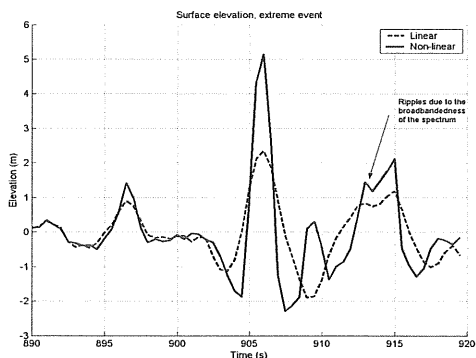


Figure 4. Non physical extreme wave above the wave-breaking limit of 5.07 meters

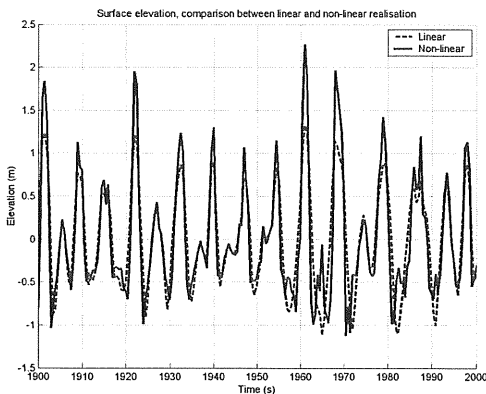


Figure 5. Surface elevation in meters. Comparison of the linear and non-linear case for waves below the wave-breaking limit.

In fig. 6 and 7 resulting force and base moment between 1900 and 2000 seconds for the same wave realisation are shown. One can see an increase in the maximum force for the non-linear realisation due to the increase in velocity and the fact that a larger part of the structure is submerged for the maximum wave height compared to the linear elevation. It can be also seen that the forces and base moments are highest at the crest of the waves.

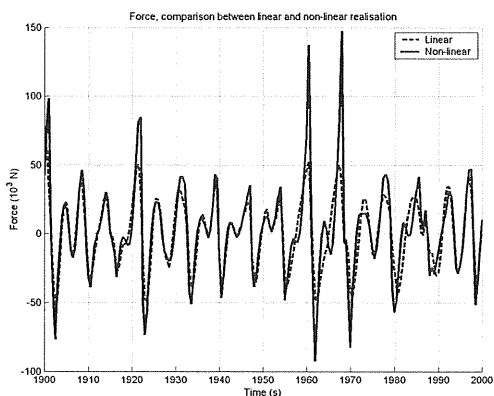


Figure 6. Force. Comparison of the linear and non-linear case for waves below the wave-breaking limit.

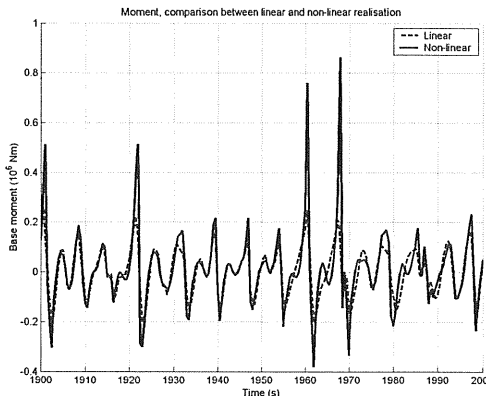


Figure 7. Moment. Comparison of the linear and non-linear case for waves below the wave-breaking limit.

Power spectra were calculated for both the linear and non-linear realisations in order to study the high-frequency contribution from the non-linear realisation.

The second-order contribution to the surface elevation is sensitive to the high frequency end of the linear input spectrum calculated in SWAN. The variation of the spectral density for the non-linear realisation is significant, fig 9. For the linear case the variation is small.

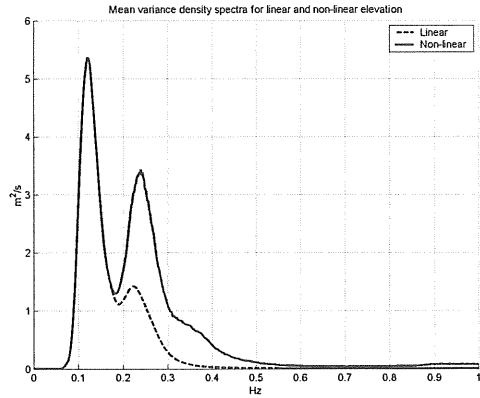


Figure 8. Mean variance density spectra for the linear and non-linear elevation.

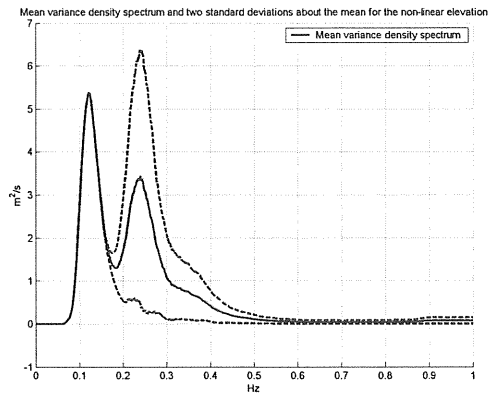


Figure 9. Mean variance density spectra and two standard deviations about the mean for the non-linear elevation.

The mean power spectra for the force and base moment are highly influenced by a time-series with a maximum wave height of 13 meters, fig. 11 and 14. The effect is enhanced by the use of Morison's equation, where the velocity is squared, and the fact that the highest velocity is at the crests of the waves. The variation in the results for the force and base moment is large, fig. 12 and 15. In figure 10 and 13 the spectra for all the time series of force and base moment are plotted and the one marked with arrows is the one with the 13 meter maximum wave height.

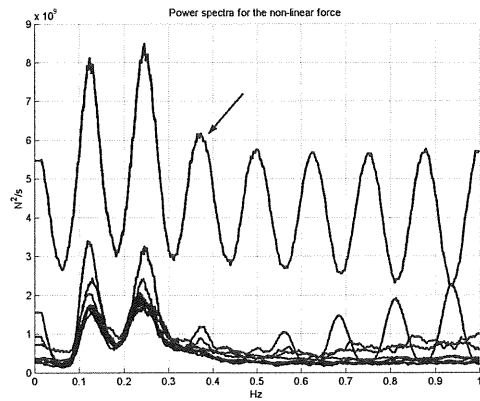


Figure 10. Power spectra for all ten time-series of the non-linear force. The spectrum marked with an arrow is from a time-series with a maximum wave of 13 meters.

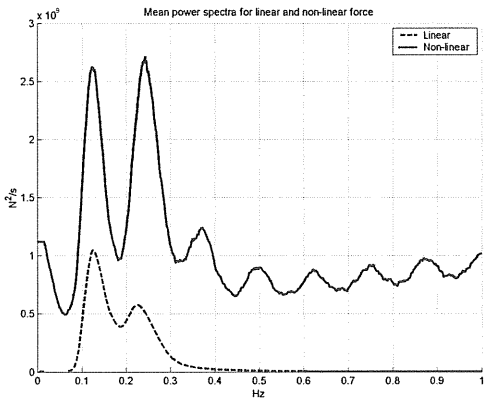


Figure 11. Mean power spectra for the linear and non-linear force.

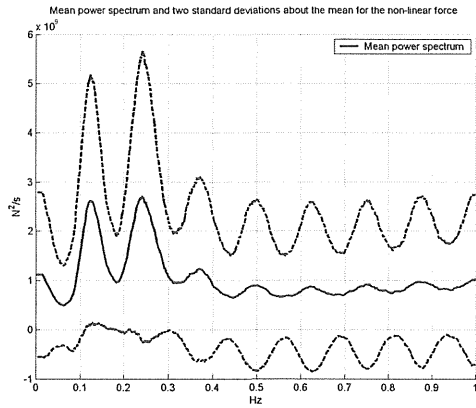


Figure 12. Mean power spectra and two standard deviations about the mean for the non-linear force.

For the base moment the influence from the time-series with the maximum wave height of 13 meters is even more pronounced, fig 14 and 15. This is due to the lever $(z + h)$ in equation 29.

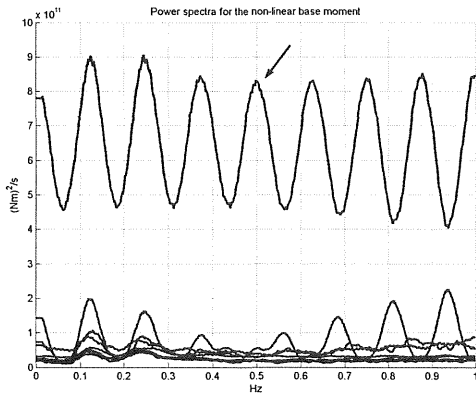


Figure 13. Power spectra for all ten time-series of the base moment. The spectrum marked with an arrow is from a time-series with a maximum wave of 13 meters.

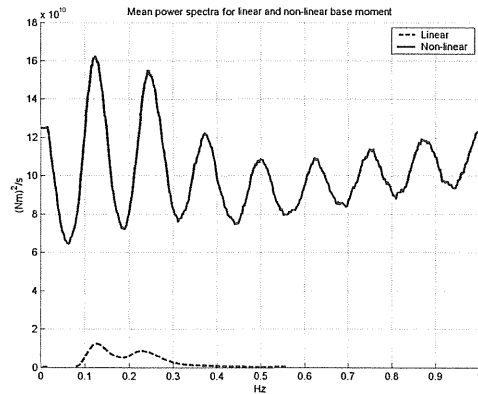


Figure 14. Mean power spectra for the linear and non-linear base moment.

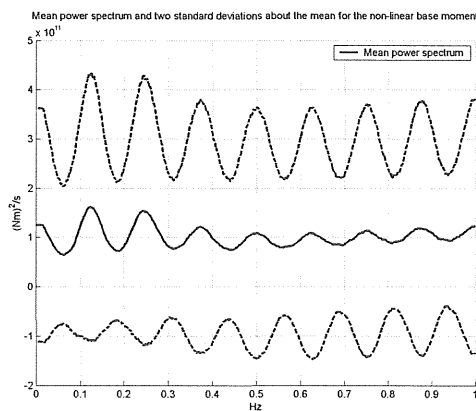


Figure 15. Mean power spectra and two standard deviations about the mean for the non-linear base moment.

The variance of the time-series increases from 0.43 to 0.69 for the water surface elevation, from $7.50 \cdot 10^8$ to $6.58 \cdot 10^9$ for the force and from $1.12 \cdot 10^{10}$ to $6.39 \cdot 10^{11}$ for the base moment.

Concluding remarks

The described method provides a way of calculating non-linear irregular waves at finite depths. However, the chosen method for calculating non-linear waves produces unrealistically high waves. A local wave steepness limiter according to Stansberg [14] will take care of some part of the problem and will also reduce the broadbandness. Stansberg [14] enforces a restriction based on keeping third-order omitted terms smaller than the corresponding second-order terms to avoid unrealistically large local wave steepness with associated velocities and accelerations, which otherwise would result in non-physical forces. This results in a restriction on the wave number and consequently on the angular frequency. The restriction can be implemented by a cut-off at the high-frequency end of the input spectrum.

In the calculation care has to be taken not to violate the limitations of the methods. It is important to test the small wave requirement of the perturbation series. A discussion on the largest wave height in water of constant depth can be found in [15]. The limiting value for H_{max} of $0.55 h$ is found to apply to shallow water waves. This is a more restrictive value than the breaker height limit $0.78 h$ for mildly shoaling bottoms used in the calculation above. The implication is that for shoaling cases $0.78 h$ should be used and for vast shallows $0.55 h$ may be more accurate but less conservative.

The wave height has to be kept beneath the wave breaking limit and one way of doing that could be to use a standard spectrum, fitted to the first peak of the non-linear SWAN spectrum, for the realisation. After the realisation is carried out a spectrum from the time-series can be constructed to be compared with the near-to-shore SWAN spectrum.

The second-order contribution is sensitive to the tail end of the linear input spectrum were the second peak is. This can further increase the variance at those frequencies for the second-order realisation.

It is observed that the calculated forces and base moments are highest at the passage of the crest of the waves. High particle velocities and the fact that a larger portion of the structure is submerged at the crest explain this. It is also observed that the non-linear realisation gives larger maximum forces and base moments than the linear realisation due to the higher wave crests.

Validation of the wave and load calculations will be carried out within the measurement program at Bockstigen. The loading on the structure has to be derived from the measured internal load effects (structural shear forces and moments), and consequently the flexibility of the structure has to be considered.

Acknowledgements

The financial support given by the Swedish Energy Agency is gratefully acknowledged.

References

1. Kühn MJ. *Dynamics and Design Optimisation of Offshore Wind Energy Conversion Systems* Ph.D. thesis; DUWIND Delft University Wind Energy Research Institute: Delft, 2001; 60-71 97-103.
2. Cheng PW. *A Reliability Based Design Methodology for Extreme Responses of Offshore Wind Turbines* Ph.D. thesis; DUWIND Delft University Wind Energy Research Institute: Delft, 2002; 17-35 43-48.
3. Cheng PW, Henderson AR. Non-linear Random Wave Loads on Support Structures of Offshore Wind Turbines. *Offshore Wind Energy in Mediterranean and Other European Seas*; Naples, Italy, April 10-12, 2003; 239-253.
4. Holthuijsen LH, Booij N, Ris RC, Haagsma IJ G, Kieftenburg ATMM, Kriezzi EE. *SWAN Cycle III version 40.11, USER MANUAL*; Delft University: Delft, 2000.
5. Wahl G. *Vågdata och vågeffekt vid svenska kustfarvatten*; Rapport 2265-3, Marintekniska institutet SSPA: Göteborg, 1983.
6. Hasselmann K. On the non-linear energy transfer in a gravity-wave spectrum, Part 1 General theory. *Journal of Fluid Mechanics* 1962; **12**:481-500.
7. Hudspeth RT, Chen M. Digital Simulation of Nonlinear Random Waves. *Journal of the Waterway Port Coastal and Ocean Division* 1979; **105**:67-85.
8. Machado UEB. *Statistical Analysis of Non-Gaussian Environmental Loads and Responses* Ph.D. thesis; Lund University of Technology: Lund, 2002.
9. Nestegård A, Stokka T. A third order random wave model. *Proc., 5th International Offshore and Polar Engineering Conference*; The Hague, The Netherlands, June 11-16, 1995; 136-142.
10. Moberg G. *Wave Forces on a Vertical Slender Cylinder* Ph.D. thesis; Chalmers University of Technology: Göteborg, 1988; 36.
11. *Shore Protection Manual, Volume 2*; Department of the Army Waterways Experiment Station, Corps of Engineers: Vicksburg, 1984; 7-103.
12. Stansberg CT. Second-Order Numerical Reconstruction of Laboratory Generated Random Waves. *Proc., International Conference on Offshore Mechanics and Arctic Engineering*; Glasgow, Scotland, June 20-24, 1993; 2:103-110.
13. *Shore Protection Manual, Volume 1*; U.S Army Coastal Engineering Research Center: Fort Belvoir, 1977; 2-121.
14. Stansberg CT. Non-Gaussian Extremes in Numerically Generated Second-Order Random Waves on Deep Water. *Proc., Eighth International Offshore and Polar Engineering Conference*; Montréal, Canada, May 24-29, 1998; 103-110.
15. Massel SR. *Ocean Surface Waves: Their Physics and Prediction*; World Scientific Publishing: Singapore, 1996; 284-305.

